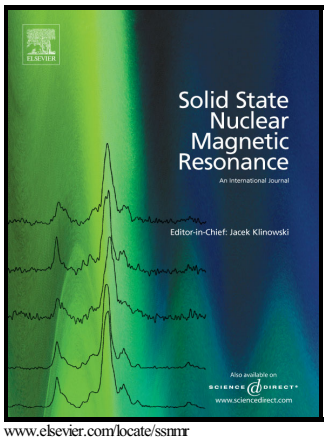

www.elsevier.com/locate/ssnmr

The effect of a broad activation energy distribution on deuteron spin–lattice relaxation

E.E. Ylinen, M. Punkkinen, A. Birczyński, Z.T. Lalowicz

PII: S0926-2040(15)30029-1
DOI: http://dx.doi.org/10.1016/j.ssnmr.2015.10.006
Reference: YSNMR718

To appear in: *Solid State Nuclear Magnetic Resonance*

Received date: 24 May 2015
Revised date: 1 October 2015
Accepted date: 7 October 2015

Cite this article as: E.E. Ylinen, M. Punkkinen, A. Birczyński and Z.T. Lalowicz, The effect of a broad activation energy distribution on deuteron spin–lattice relaxation, *Solid State Nuclear Magnetic Resonance,* http://dx.doi.org/10.1016/j.ssnmr.2015.10.006

The effect of a broad activation energy distribution on deuteron spin–lattice relaxation

E.E. Ylinen [a,*], M. Punkkinen [a], A. Birczyński [b], Z.T. Lalowicz [b]

[a] Wihuri Physical Laboratory, Department of Physics and Astronomy, University of Turku, FI-20014 Turku, Finland

[b] H. Niewodniczański Institute of Nuclear Physics of PAS, ul. Radzikowskiego 152, 31-342 Kraków, Poland

*Corresponding author
Dr. Eero Ylinen
Wihuri Physical Laboratory, Department of Physics and Astronomy
University of Turku, FI-20014 Turku, Finland
E-mail address: eero.ylinen@utu.fi

Abstract

Deuteron NMR spectra and spin–lattice relaxation were studied experimentally in zeolite NaY(2.4) samples containing 100 % or 200% of CD_3OH or CD_3OD molecules of the total coverage of Na atoms in the temperature range 20 K – 150 K. The activation energies describing the methyl and hydroxyl motions show broad distributions. The relaxation data were interpreted by improving a recent model [Solid State Nucl. Magn. Reson. 49−50, 33–41 (2013)], in which the nonexponential relaxation curves are at first described by a sum of three exponentials with adjustable relaxation rates and weights. Then a broad distribution of activation energies (the mean activation energy A_0 and the width σ) was assumed for each essentially different methyl and hydroxyl position. The correlation times were calculated from the Arrhenius equation (containing the pre-exponential factor τ_0), individual relaxation rates computed and classified into three classes, and finally initial relaxation rates and weights for each class formed. These were compared with experimental data, motional parameters changed slightly and new improved rates and weights for each class calculated, etc. This method was improved by deriving for the deuterons of the A and E species methyl groups relaxation rates, which depend explicitly on the tunnel frequency ω_t. The temperature dependence of ω_t and of the low–temperature correlation time were obtained by using the solutions of the Mathieu equation for a threefold potential. These dependencies were included in the simulations and as the result sets of A_0, σ and τ_0 obtained, which describe the methyl and hydroxyl motions in different positions in zeolite.

Key words: non-exponential NMR relaxation; activation energy distribution; decreasing activation energy; rotational tunnelling; methanol in zeolite; deuteron NMR spectra; molecular mobility; methyl group; hydroxyl group

1. Introduction

Deuteron NMR spectrum and spin–lattice relaxation are widely used for studying structural and motional properties of solids. Of special interest have been the samples containing deuteron tetrahedra or CD_3 groups at low temperatures, where rotational tunnelling changes spectra and relaxation in a characteristic way [1−11]. The presented models agree usually well with experimental results for single crystals of such materials.

Spectra and relaxation become more complicated to analyse if the activation energy for the motion of CD_3 or deuteron tetrahedron shows a broad distribution. Then the line-width transitions extend over a much larger temperature range than in the absence of the distribution. Similarly the normal maxima of the relaxation rate as a function of temperature, corresponding roughly to $\omega_0\tau = 1$ (ω_0 is the deuteron resonance frequency and τ the correlation time of the dominant motion), become nearly flat. Since there is practically no spin diffusion between deuterons in solids, the relaxation appears highly nonexponential so that in principle an enormous number of exponential functions $\exp(-Rt)$ is needed to describe the magnetization recovery accurately. Of course some nonexponentiality can be related to the orientation dependence of the involved transition rates, and in the case of weakly hindered methyl groups rotational tunnelling may complicate the relaxation additionally. In general the orientation dependence remains hidden under the influence of the activation energy distribution, and the effect of tunnelling is considered in detail later on in this study. There are several methods for analysing the deuteron spectra for such CD_3 containing samples [12−15]. However, the analysis of relaxation results for broad distributions was not possible until recently because of a lack of reliable methods. Cereghetti et al. [13] introduced a method, which is valid for roughly equivalent methyl groups, which anyway show a significant distribution of activation energies. Recently Stoch et al. [16] presented a model, which can be applied in samples, where there are two or more distinctly different CD_3 positions. In such a case the methyl groups in one kind of position are roughly equivalent, but because of their different surroundings for example in zeolites they can anyway show a broad distribution of motional activation energies, while the mean activation energies for different positions may deviate from each other more than the distribution widths. The model was applied to methyl and hydroxyl groups of methanol molecules in zeolite NaX.

The mentioned method [16] is an experiment–based model, which needs a quite accurate description of the observed magnetization recovery. It was done by using a sum of three exponentials with adjustable weights and characteristic relaxation rates R_f, R_m and R_s for the fast, intermediate and slow components, respectively. Two exponentials cannot in general reproduce the observed recovery with sufficient accuracy. In principle the number of exponentials could be four or even five, but in practice such an increase is limited by the fact that for a growing number of exponentials the scatter in weights and characteristic rates becomes too large. The so-called stretched-exponent function $\exp[-(t/T_c)^x]$ would probably produce good fits, but so far there is no theoretical method for calculating the time constant T_c. Therefore we chose to use three exponentials. The success of such fits is demonstrated for example by Fig. 1 of Ref. [16].

For each distinctly different position of CD_3 a Gaussian distribution was introduced with the mean activation energy A_0 and the distribution width σ. When the pre-exponential factor τ_0 is defined, a numerical value R_j is calculated for each point j of the

relevant distribution from the well-known expression for the relaxation rate in polycrystalline samples [5, 16, 17]

$$R_{\mathrm{j}} = \frac{\omega_{\mathrm{Q}}^2}{15}\left[\mathrm{J}\left(\tau_{\mathrm{j}}, \omega_0\right) + 4\mathrm{J}\left(\tau_{\mathrm{j}}, 2\omega_0\right)\right] \qquad (1)$$

Here $\omega_{\mathrm{Q}} = \mathrm{e}^2\mathrm{qQ}/\hbar = 2\pi\nu_{\mathrm{Q}}$ and τ_{j} is the correlation time of the 120° jumps about the methyl axis for the activation energy $A_0 + \Delta A_{\mathrm{j}}$ of the distribution. τ_{j} is obtained from the Arrhenius equation

$$\tau_{\mathrm{j}} = \tau_0 \exp\left[\left(A_0 + \Delta A_{\mathrm{j}}\right)/\mathrm{R}T\right] \qquad (2)$$

The spectral density functions are defined by $\mathrm{J}\left(\tau_{\mathrm{j}}, \omega\right) = \tau_{\mathrm{j}}/\left(1 + \omega^2\tau_{\mathrm{j}}^2\right)$. The calculated rates R_{j} are classified into three classes by comparing them to the limiting quantities $\sqrt{R_{\mathrm{f}}R_{\mathrm{m}}}$ and $\sqrt{R_{\mathrm{m}}R_{\mathrm{s}}}$. The distribution–related weight of the point j is $\mathrm{w_j} = \exp\left(-\Delta A_{\mathrm{j}}^2/2\sigma^2\right)/\sum_{\mathrm{j}}\exp\left(-\Delta A_{\mathrm{j}}^2/2\sigma^2\right)$. Then the initial relaxation rate for each class c (= f, m or s) is calculated from

$$R_{\mathrm{ci}} = \sum_{\mathrm{j}'} \mathrm{w_{j'}}\, R_{\mathrm{j}'}/\sum_{\mathrm{j}'} \mathrm{w_{j'}} \qquad (3)$$

where the prime in the summation index j' means that for example the relaxation rate of the intermediate class m depends only on those $R_{\mathrm{j}'}$ values which obey $\sqrt{R_{\mathrm{f}}R_{\mathrm{m}}} > R_{\mathrm{j}'} > \sqrt{R_{\mathrm{m}}R_{\mathrm{s}}}$. The obtained quantities R_{ci} are compared with the experimental rates R_{f}, R_{m} and R_{s} at each temperature and the parameters A_0, σ and τ_0 are then adjusted to obtain better values for R_{ci}. This cycle is repeated many times to obtain the optimal fit. The initial relaxation rates R_{ci} are used because they are easy to compute. It would be more correct to use the average relaxation rate for each class. According to our estimates R_{ci} is larger than the corresponding average rate by a factor varying between 1.1 (the fast component) and 2.0 (the slow component) [16]. Since we are mainly interested in the temperature dependence of the rates and weights, the difference between the initial rates R_{ci} and the average rates is not of critical importance.

The description above is valid when the methyl groups are located at one kind of position only. If there are two or more distinctly different position, then for each position another set of the parameters A_0, σ and τ_0 are needed and the iteration cycle has to take into account the corresponding relaxation rates. Furthermore, the sample may contain deuterons outside methyl groups, which can be taken into account similarly by replacing the expression (1) by a relevant one.

This model was used to explain the experimental data on deuteron spin–lattice relaxation in three samples of zeolite NaX(1.3), which contained 100 % or 200 % of CD_3OH or CD_3OD in comparison with the total Na^+ concentration [16]. The obtained agreement between the model and experimental data was reasonable. These experiments covered the temperature range from 20 K to T_{S} = 167 K. T_{S} means the temperature, below which the methanol molecules are localized at certain equilibrium positions, numbered I, II, etc. in the following. Two such positions are significantly occupied in NaX [16], while a third position is also occupied in NaY (Section 3). Above T_{S} methanols become free to move and the rotational motion becomes effectively isotropic.

The deuteron relaxation of heavy methanol molecules was also studied in NaX and NaY above T_S [15]. Actually the NaY sample was the same as Sample 3 of this study (Section 3) and for it T_S = 154 K. In both these zeolites the deuteron relaxation between T_S and 300 K was observed to be biexponential. The faster relaxation rate, related to the hydroxyl deuterons, is about 9 times the slower rate corresponding to the CD_3 deuterons in the entire temperature range. Effectively isotropic reorientation (at higher temperatures translation) is the dominant motion for both the OD and CD_3 groups, but its effectiveness in the CD_3 relaxation is reduced by even faster rotation about the methyl axis. Just above T_S there is a narrow transition region where the dominant motion of relaxation changes from effectively isotropic reorientation of methanols to the internal motion of localized molecules [16]. Below T_S the methanol molecules remain localized and their reorientation becomes nonisotropic or stops practically completely. Still the methyl groups rotate about their threefold axis and the OD vectors undergo some restricted motion about their equilibrium orientation. These motions are responsible for the deuteron relaxation below T_S in NaX [16] and in NaY samples of the present study.

Although the presented model explains reasonably well the NaX experiments [16], there are some deviations, which may at least partly originate from the fact that the model did not take into account two features: (i) In the case of very small activation energies the potential hindering the methyl rotations is so low that the rotational tunnel splitting ω_t can be equal or even larger than the deuteron resonance frequency ω_0 [18]. In such a case Eq. (1) is no more valid. (ii) It has been observed that at low temperatures the rotational correlation time cannot be obtained from the Arrhenius equation by using one constant activation energy but the apparent activation energy decreases [19, 20]. In carboxylic acid dimers the hydrogen correlation time becomes practically constant [21].

These two factors are taken into account in the present study. In Supplemental Material we derive coupled differential equations governing the deuteron magnetizations M_A and M_E, corresponding to the CD_3 groups with the spin and rotational wave functions belonging to the irreducible representations A and E (= E^a and E^b) of the point group C_3, respectively. For the initial relaxation rates of these magnetizations we derive expressions, which depend on the tunnel frequency ω_t and replace Eq. (1).

The rotational energies for a one-dimensional rotor like CD_3 can be calculated from the so-called Mathieu equation as the function of the height of the potential hindering methyl rotation (Section 2). From the energy eigenvalues we can calculate the tunnel frequencies and the average rotational energies for the excited rotational states, which are then used to evaluate the temperature variation of the observed tunnel frequency, needed in the numerical calculations of the relaxation rates of M_A and M_E. For the other important factor, the temperature dependence of the rotational correlation time, we use a combination of the models by Stejskal and Gutowsky [22], Müller-Warmuth et al. [20] and Clough et al. [23].

In Section 3 at first experimental details and the methanol containing NaY samples are presented. Then some experimental deuteron spectra are shown and discussed. These are important for the application of the described model on the deuteron relaxation. The results of relaxation experiments are shown and explained in detail in Section 4. The last section discusses the advantages and weaknesses of the used model.

2. Deuteron relaxation and correlation time

2.1. CD_3 tunnel splitting and correlation time at low temperatures

In Supplemental Material we show that the populations of the A and E species CD_3 groups can be reasonably well described by two spin temperatures T_A and T_E. We derived the initial relaxation rates for the corresponding magnetizations M_A and M_E after the saturation by a 90° pulse (S12) (Supplemental Material). The rates depend on two coherence damping rates k_K and k_t. They are roughly equal at high temperatures but k_t becomes increasingly larger than k_K when temperature is lowered [24, 25]. Partly to reduce the number of parameters, partly to simplify numerical calculations in general, we use only one damping rate $k_K = k_t = 1/\tau$, which is equal to the inverse of the corresponding correlation time τ. Then the spectral density functions $S(k,\omega)$ in Eqs. (S5) and (S6) become equal to the functions $J(\tau,\omega)$ in (1). For polycrystalline samples the initial relaxation rates (S12) simplify then to

$$R_{\mathrm{Ain}} = (1/30)\omega_Q^2[\mathrm{J}(\tau,\omega_t+\omega_0)+\mathrm{J}(\tau,\omega_t-\omega_0)+4\mathrm{J}(\tau,\omega_t+2\omega_0)+4\mathrm{J}(\tau,\omega_t-2\omega_0)]$$

$$R_{\mathrm{Ein}} = (1/120)\omega_Q^2[6\mathrm{J}(\tau,\omega_0)+\mathrm{J}(\tau,\omega_t+\omega_0)+\mathrm{J}(\tau,\omega_t-\omega_0)+24\mathrm{J}(\tau,2\omega_0)$$
$$+4\mathrm{J}(\tau,\omega_t+2\omega_0)+4\mathrm{J}(\tau,\omega_t-2\omega_0)] \qquad (4)$$

If the tunnel frequency ω_t is much smaller than the resonance frequency ω_0, the rates R_{Ain} and R_{Ein} both reduce to the well-known equation (1). Under such conditions the motion–dependent part of the secular quadrupole Hamiltonian tends to equalize the E^a and E^b level populations and the spin temperatures T_A and T_E (Table SI) (Supplemental Material). Nevertheless, in the fast-motion limit $\omega_0\tau < 1$ the magnetizations M_A and M_E are coupled to the so-called rotational polarization (= the population difference between the E^a and E^b levels). In the following we ignore this coupling and use still the relaxation rates (4). For weakly hindered methyl groups at low temperatures the tunnel frequency ω_t may exceed ω_0. Then the relaxation should be practically biexponential, the rates being nearly equal to R_{Ein} and R_{Ain} [see Eqs. (S8) and (S9)]. When the tunnel and resonance frequencies are near each other, the couplings between M_A and M_E and to the tunnelling reservoir may make the true eigenrates differ more from the initial relaxation rates as described in Supplemental Material. This error is corrected qualitatively by requiring that when calculating R_{Ain} the differences $|\omega_t - \omega_0|$ and $|\omega_t - 2\omega_0|$ in the denominators of the resonant rates like $R_{\mathrm{ta-1}}$ and $R_{\mathrm{ta-2}}$ (S6) are never allowed to be smaller than $\omega_0/2$. In the case of broad activation energy distributions the relative number of CD_3 groups with ω_t and ω_0 nearly equal is expected anyway to be rather small, therefore this replacement, which is only qualitatively right, should not cause significant errors in final fits. Simulations showed that the use of the corrected R_{Ain} instead of the uncorrected one caused only insignificant changes. Thus the nonexponential relaxation in the level-crossing region can be described by two exponential functions. But neither of these exponentials represents A nor E species deuterons, actually the exponentials represent a combination of them. Instead of saying that the deuterons of the A and E groups relax biexponentially we can say that a part of

the deuteron magnetization of these groups relaxes exponentially at the rate R_{Ain} and the remaining part at the rate R_{Ein}. Consequently we are able to describe the deuteron relaxation in the entire experimental temperature range, before taking into account the activation energy distribution, by the initial rates (4). These represent a clear improvement relative to Eq. (1) used in our previous study [16] although they remain somewhat semiquantitative especially in the level-crossing region.

The rates (4) depend strongly on the tunnel frequency ω_t, which varies with temperature. To estimate its temperature dependence we solved the Mathieu equation [18]

$$\left[-\frac{\mathrm{B}\mathrm{d}^2}{\mathrm{d}\phi^2}+\mathrm{V}(\phi)\right]\mathrm{R}(\phi)=\mathrm{E}\,\mathrm{R}(\phi) \qquad (5)$$

Here R(ϕ) is a rotational eigenfunction, E the corresponding energy and B the rotational constant equal to 0.327 meV for CD_3. We use the purely threefold potential V(ϕ) = $(V_3/2)(1 - \cos 3\phi)$, where V_3 is the height of the barrier. The rotational functions can be expressed as $\mathrm{R}(\phi) = \Sigma_n\, g_n\, e^{i(\delta+3n)\phi}$, where δ = 0, 1 and 2 for the A, E^a and E^b states, respectively. A recursion formula is derived for the multipliers g_n. Converging rotational functions are obtained only for discrete values of E_{rs}, which are the desired energy eigenvalues. The subindex r defines the rotational state and s refers to A, E^a or E^b.

All the energy eigenvalues, up to the sixth excited state, were calculated for evenly distributed potential heights, starting from $V_3/2B = 10$ up to 180, the step being 5. For the r^{th} excited rotational state we use the mean energy $E_r = (E_{rA} + E_{rEa})/2$ and the tunnel frequency $\omega_{rt} = (E_{rEa} - E_{rA})/\hbar$. The conventional activation energy was taken equal to the difference $A_0 = V_3 - E_0$. We call the corresponding differences $A_r = E_r - E_0$ for excited rotational states also activation energies. These make it possible to estimate the temperature dependence of the observed tunnel frequency ω_t. For this purpose the following somewhat semiquantitative expression is widely used

$$\omega_{\mathrm{t}} = \textstyle\sum_{\mathrm{r}} \omega_{\mathrm{rt}} \exp(-A_{\mathrm{r}}/\mathrm{R}T) / \sum_{\mathrm{r}} \exp(-A_{\mathrm{r}}/\mathrm{R}T) \qquad (6)$$

ω_t is practically constant at low temperatures, starts to decrease when T is raised, then there is an inflexion point after which the rate of decrease slows down. The temperature dependence was calculated from (6) up to the inflexion point and then the function $\omega_{\mathrm{t}} = \omega_{0\mathrm{t}}/(1 + \alpha T^{\beta})$ fitted to the obtained points. This function has been observed to describe the experimentally observed points quite well [26]. Furthermore, it depends only on two parameters α and β and is therefore fast to compute in comparison with (6), which requires the inclusion of many excited states especially at high temperatures. The parameters α and β are shown as a function of the activation energy A_0 in Fig. 1.

At relatively high temperatures most rotational jumps take place over the barrier. At lower temperatures jumps at excited rotational states become more significant and the activation energies A_r are used to describe them. At each such level the jumps are assumed to occur at a rate proportional to $|\omega_{\mathrm{rt}}| \exp(-A_{\mathrm{r}}/\mathrm{R}T)$ according to the Arrhenius equation. This proportionality was proposed already by Stejskal and Gutowsky [22]. Of course the relaxation rates should be related to the time-dependent phonon–rotation coupling and not to the time-independent potential V(ϕ), therefore their model cannot be true in principle. Nevertheless, it leads to a quite good agreement with experiment as shown by numerical calculations by Clough et al. [23].

Furthermore, by using it there is no need to introduce new parameters. Therefore we use it here to describe the temperature dependence of the correlation time at low temperatures. Similarly, the rate of the jumps over the barrier is taken proportional to $|\omega_{bt}|\exp(-A_0/RT)$, where $|\omega_{bt}|$ is the tunnel frequency for such an excited energy $E_r = (E_{rA} + E_{rEa})/2$, which is equal to the barrier height V_3. Finally we include in the calculations two parameters K_h and K_l and express the total rotational jump rate as

$$1/\tau = K_h|\omega_{bt}|\exp(-A_0/RT) + K_l\sum_r|\omega_{rt}|\exp(-A_r/RT) \quad (7)$$

Fig. 2 presents the activation energies $A_r = E_r - E_0$ of the excited states and the normal high-temperature activation energy $A_0 = V_3 - E_0$ (this is naturally a straight line) as the function of A_0. The curve (nearly straight line) below the horizontal axis represents $-E_0$ and thus shows the bottom of the potential V(ϕ). So the vertical distance between the straight line and the nearly straight line below the horizontal axis is always equal to V_3. Fig. 3 describes the variation of the absolute values of the tunnel frequencies $|\omega_{rt}|$ for various excited states. For most of the curves in Figs. 2 and 3 the calculated values fall very exactly on the curves and are therefore not shown. The only exception is ω_{bt}, for which the calculated results show considerable scatter (Fig. 3). When calculating numerical estimates for the correlation time τ from (7) the excited states were taken into account only when the rotational energy $E_r = (E_{rA} + E_{rEa})/2$ is smaller than the potential height V_3.

2.2. Relaxation of OD deuterons

The spin−lattice relaxation of the OD deuterons is not so reliably understood, since the hydroxyl motion is not known in detail. In NaX the methanol molecules were assumed to be situated at the positions I and II in the zeolite framework [16]. In the former position (called horizontal) the methanol oxygens are bonded to the sodium ions, and in the latter (called vertical) the methanols are hydrogen−bonded to the oxygens in the zeolite framework [15, 27]. In NaY we assume also a third position (or structure) III, where additional methanols form hydrogen bonds via their oxygen to the OD group of methanols in position I (Fig. 4). This way a second (and third, etc.) adsorption layer is formed as proposed before (structure V in the Scheme I [27]).

In the previous study it was assumed that the O–D vector is more free to move in position I than in II, because in the latter position the hydrogen bonding restricts deuteron motion [16]. The O–D motion in position I was assumed to occur by small angles about the equilibrium orientation. The angle is expected to become larger with temperature. Thus both the motional angle and rate vary with temperature. These processes were described by a model called limited jumps, in which the O–D vector moves (with the temperature dependent rate $1/\tau_{lj}$) on the cone making the angle Δ with the equilibrium orientation at low temperatures. The corresponding relaxation rate for the point j of the activation energy distribution is [9, 16]

$$R_{lj}(j) = E\frac{\omega_Q^2}{15}\left[J\left(\tau_{lj}(j), \omega_0\right) + 4J\left(\tau_{lj}(j), 2\omega_0\right)\right] \quad (8)$$

This is formally identical to Eq. (1) describing the relaxation of methyl deuterons for methyl groups rotating about their axis, the only difference is the efficiency factor E. Because now the motional angle is smaller than the tetrahedral angle, the relaxation rate is reduced to $E = (27/32)(4\sin^2\Delta\cos^2\Delta + \sin^4\Delta)$.

At higher temperatures it is possible that the O–D vector of the methanol molecule jumps to a totally different direction by a 120° jump about the C–O vector. Such a jump is analogous to the motion of the C–D vectors when the methyl group rotates about its axis. This hydroxyl rotation modulates the quadrupole interaction of hydroxyl deuterons, and the corresponding relaxation is again analogous to Eq. (8), but with the different efficiency 1 – E instead of E, since a large part of the relaxing power of the quadrupole interaction is already used by limited jumps.

The limited–jump part (corresponding to Eq. (8)) is used to describe the relaxation of hydroxyl deuterons in position I roughly up to 80 K. However, we assume now that only the angle Δ grows with temperature while the correlation time τ_{lj} is practically constant (but still shows a reasonable distribution). The latter assumption is understandable, when we realize that limited jumps here means O–D vectors vibrating about the equilibrium orientation, similarly to lattice vibrations, which have frequencies practically independent of temperature. To describe the temperature dependence of E, we use here for it an alternative expression $E = q \exp(-T_{lj}/T)$. The parameters q and T_{lj} are defined later on.

When T approaches T_S, the methanols start to move more isotropically. Then limited jumps is no more a dominant motion. Here this change is taken into account by ignoring the direct contribution of the limited–jumps to the relaxation when the 120° rotations of hydroxyl vectors start to dominate. This seems to happen near 80 K. The jumps are anyway assumed to reduce the relaxing efficiency of the hydroxyl rotation, 1 – E. Thus the takeover temperature depends also to some extent on the limited–jump angle Δ. Since the hydroxyl rotation really contributes to the relaxation, 1 – E must always be larger than zero. Therefore E has to remain smaller than 1 even above 100 K. This is achieved by requiring that E increases with temperature up to a certain temperature T_E and remains then constant.

Similarly to the previous study we assume the OD(II) deuterons to relax at temperature−independent rates, showing anyway a certain distribution [16]. This description is consistent with the limited jumps model (8) when both the jump rate and angle are constants. Because the hydroxyl in positions II are hydrogen–bonded to the framework oxygens, their vibration should be much more restricted than that of hydroxyls I, which makes the constant-angle assumption easier to understand. Most probably the relaxation rates of OD (II) are not exactly constant but start to grow when temperature is raised towards T_S (Fig. 10). The relatively small effect of hydroxyl deuterons to the relaxation and the limited accuracy of the experimental points and of our analysing methods make useless any efforts to find better models.

Concerning the relaxation of the OD(III) deuterons, we do not find any clear experimental or theoretical information for the detailed description of their dominant motion. Therefore, we use Eq. (8) for the corresponding hydroxyl deuterons with the same parameters as for OD(I). This way no additional parameters are needed. Still the methyl motions in these positions are assumed to be different.

3. Experimental details and deuteron spectra

Our samples of methanol containing zeolite NaY(2.4) were prepared in the same way as described in the previous study [15]. They contain 100 % and 200 % of CD_3OH (Samples 1 and 2, respectively) and 200 % of CD_3OD (Sample 3) of the total coverage of Na^+ ions. All the samples were sealed in 24 mm long glass tubes with the outside

diameter 5 mm. Experiments to be described were carried out mainly below the temperature T_S = 154 K, where the methanols are localized [15].

Experiments were carried out at the deuteron resonance frequency 46 MHz. The resonance signal was observed by the quadrupole echo, with a 200 μs delay between the two pulses [15]. The experimental signals were phase-corrected and Fourier–transformed to obtain the deuteron spectra. In relaxation experiments the quadrupole echo sequence was preceded by a short burst of $\pi/2$ pulses, which saturated the magnetization. The delay between the saturation and echo sequences was varied to facilitate the observation of the recovery curve.

Just above T_S there appears a narrow central component in the otherwise broad deuteron spectrum. Its intensity grows rapidly at higher temperatures at the expense of broader components, showing the ability of methanols to become free from the equilibrium positions, at first for short times. This is true when the sample temperature is lowered stepwise from high temperatures towards T_S. If temperature is gradually raised through T_S, the mentioned changes start to take place at a somewhat higher temperature. This shows that there is some hysteresis in the process of becoming free to move off from the bonding positions I−III. In the following we do not pay much attention to the spectra for $T > T_S$ because our main interest is the internal motions and related activation-energy distributions of localized molecules below T_S.

Fig. 5a shows the deuteron spectrum at 5 K for Sample 1. Since this sample does not contain any hydroxyl deuterons, the entire spectrum is related to the methyl deuterons. The doublet dominating the spectrum is composed of (i) the doublet representing methyl groups, which rotate about the methyl axis faster than the quadrupole frequency ω_Q, and of (ii) the tunnelling–related spectrum arising from methyl groups with $\omega_t > \omega_Q$ (but rotating at a frequency smaller than ω_Q). In the latter contribution the doublet is accompanied by the characteristic sideband [3, 4]. The theoretical spectra for both these components were calculated with the quadrupole frequency $\nu_Q = \omega_Q/2\pi$ = 150 kHz and their respective contributions are 43 % and 30 %. The experimental spectrum contains also two Pake doublets, characterized by ν_Q = 94 and 175 kHz, with respective contributions 16% and 11 %, related to immobile deuterons in methyl groups. The spectrum of Sample 2 (Fig.5b) is composed of similar subspectra: (i) rotating and (ii) tunnelling components, one Pake doublet (ν_Q = 175 kHz) and a Gaussian with the respective contributions 50 %, 10 %, 22 % and 18 %. We attribute the Gaussian component to deuterons undergoing large-scale oscillations in space leading finally to a narrow line for isotropic reorientations at high temperatures.

In zeolites NaX containing methanol molecules the spectral features were related to certain positions (also called structures) of adsorbed methanol molecules [16]. In NaY samples we adopt a similar approach, although we now need also the third structure III. Some support for this structure is provided by the differences between NaX and NaY. There are 86 sodium cations in the unit cell of NaX, 32 of them are located at positions SII in the supercage, 32 at SI'at the window of the hexagonal prism, and remaining 22 at position SIII in the supercage [28, 29]. Thus 54 of all sodiums are available for methanols in supercages as structure I. Most, if not all methanol molecules are expected to be located in supercages. At 100% loading remaining 32 may be found as structure II. In zeolite NaY site SII is the preferred one and fully populated, close to the maximum of 32 from the total number of 56 for Si/Al = 2.4. The rest of cations, namely 24, are distributed between positions SI and SI', as position SIII is hardly populated. Positions of sodium cations are shown in Fig. 1 of Ref. 30. Many factors may perturb this situation, particularly the presence of adsorbed molecules. Their presence tends to transfer cations toward the supercage, even more effectively when the adsorbed

molecules are polar [31, 32].

Furthermore, there are differences in the neutralization of the electric charge of sodium cations by oxygen framework atoms. The extent of neutralization is smaller in NaY and the electrical charge of Na^+ is higher, leading to a stronger bonding of methanol molecules at position I. On the other hand, framework oxygen atoms are less negative in NaY than in NaX (due to a smaller number of AlO^-_4 tetrahedra in the unit cell), and the hydrogen bonding at position II is weaker. The unit cell of zeolite Y contains 384 oxygen atoms at four crystallographically inequivalent positions from O1 to O4.

As about assignment of spectral components to structures we propose the following picture. A relatively smaller fraction of the positions at sodium cations is available for methanol molecules in NaY than in NaX. Some may be not accessible and therefore we take into account also structure III. In Sample 1 (Fig.5a) the tunnelling component (contribution 30%) may be attributed to methanol molecules in the structure II. Contribution of rigid deuterons amounts to 27% and may be presumably related to the structure I. Some methyl groups at position I may still rotate and, together with the methyl groups of the structure III, produce the rotating component with the 43% contribution. In Sample 2 (Fig.5b) we may assume equal populations of methanol molecules (and of methyl groups) over the three structures I – III. This leads to the following assignments: Tunnelling component (with 10% contribution) corresponds to 1/3 of the methanol molecules at positions II, Gaussian (18%) to practically 2/3 of the methanols II, and rigid (22%) to 2/3 of the methanols I. The rotating component consists of 1/3 of the methanols I and all the methanols III (experimental contribution 50%, from the assignment above 44%). The differences between the experimental and model-based results may be related to motional perturbation of molecules in structures I and II due to a higher abundance of molecules in the second layer.

Representative spectra for Sample 3 are shown in Fig. 6 for low temperatures below T_S. Spectra evolve from the existence of tunnelling at low temperatures to the appearance of a small narrow component due to effectively isotropic reorientation of some methyl groups near T_S. More insight into the details of the temperature dependence of the spectra of Sample 3 is provided by Fig. 7, which shows the relative contributions of all the spectral components as a function of inverse temperature. The tunnelling–related component decreases above 20 K and is not observed above 40 K. The Pake doublets decrease above 40 K and reach a constant value at 63 K. Simultaneously the component assigned to rotating methyl groups grows and reaches a maximum at 91 K. At higher temperatures the rotating component starts decreasing due to the appearance of a new doublet with a smaller effective quadrupole coupling. It originates probably from hydroxyl groups performing rotation about a pseudo-threefold axis, making an angle smaller than tetrahedral with the O–D direction. The contributions of the various components are practically constant between T_S and 200 K, and the narrow central component does not yet have a significant amplitude. This is understandable because these results were observed by increasing temperature stepwise from below T_S. Because of the hysteresis the methanol molecules are still practically localized. When the number of methanol molecules in structure III is assumed to be equal to those of structures I and II, the methyl and hydroxyl deuterons at any one of these structures contribute 25 % and 8.33 % of the total spectral area, respectively. The variation with temperature of the spectral components and their relation to the three structures is described in Table I. The numerical contributions in the brackets, based on equal occupation of the positions I – III, agree well with the experimental values.

All this is consistent with a distribution of the potential strength due to subtle

differences in the bonding to supercage walls. There is also a marked difference to zeolites containing heavy methane instead of methanol molecules. CD_4 molecules experience only negligible bonding to zeolite and between each other. Therefore they are practically free to move, what leads to a narrow spectrum even at low temperatures [33].

Our results provide also some data on the value of the quadrupole coupling constant of deuterons in methanol molecules. The coupling constant for the methyl group may adopt slightly different values depending on the local electronic structure of a given molecular system. In aspirin single crystal it equals 160 kHz [4], while analysis of spectra for CD_3CH_2OH in nematic solvents provides 180.7 kHz [34]. We obtained 150 kHz.

Let us consider a set of Pake doublets corresponding, in NMR terminology, to immobile deuterons, which are bonded to framework oxygens. The observed effective quadrupole coupling constant is the vector sum of internal and external electric field gradients at the deuteron. We find the following coupling constants at low temperature (relative contributions are given in brackets): 100 kHz (7%), 175 kHz (18%), 210 kHz (9%) and 240 kHz (11%). The first two values correspond well to Pake doublets in Fig.5a. Therefore, we can attribute these values to methyl group deuterons of the structure I. At high temperature we have Pake doublets characterized by the following parameters: 185 kHz (3%), 205 kHz (3%) and 232 kHz (3%) all related to the hydrogen–bonded deuterons of the methanol hydroxyl groups in the structure II. A similar set of quadrupole coupling constants was derived for methanol molecules in NaX at low temperature [15]. Comparable values were obtained for D_2O molecules at 100 % loading in NaY at low temperature [35]. Deuterons in bridging hydroxyl groups in DY zeolite provide the following values of the quadrupole coupling constant: 130, 170 and 212 kHz and an assignment to framework oxygens was proposed [36].

4. Experimental relaxation data and simulations

4.1. Deuteron relaxation in Sample 2

We show and discuss first the experimental relaxation data for Sample 2 containing 200 % of CD_3OH, since there are no hydroxyl deuterons in it and therefore the application of our model is easier. Furthermore, the relaxation results for Samples 1 and 2 were nearly identical within the experimental scatter, so there is no need to discuss them separately. The function $M_z(t) = \sum_{i=1-3} M_i[1 - \exp(-R_i t)] + c_0$ was fitted to the magnetization recovery by varying the relaxation rates R_i and the amplitudes M_i by the least-squares method. The parameter c_0 may have a nonzero value if the saturation is not perfect. The relative weights w_i are calculated from the amplitudes M_i, for example $w_1 = M_1/(M_1+M_2+M_3)$. The obtained relaxation rates and weights are shown in Figures 8–11 for samples 2 and 3.

The relaxation rates of the three exponentials increase at first sharply when temperature is lowered below T_S, show then a plateau or maximum, and finally start to decrease (Fig. 8). The weight of the fast-relaxing component decreases at first, then increases strongly to the maximum near 50 K, and finally decreases at still lower

temperatures. The weight of the intermediate component decreases steadily with temperature while that of the slow component shows a minimum near 50 K (Fig. 9). The relaxation rates for Sample 3 differ from those of Sample 2 by a minimum, which appears between 70 and 90 K in all the three components (Fig. 10). The weight of the fast component in Sample 3 behaves similarly to that of Sample 2, but the variations in the weights of the intermediate and slow components are larger than in Sample 2 (Fig. 11).

For numerical simulations the limiting values $L_{fm} = \sqrt{R_f R_m}$ and $L_{ms} = \sqrt{R_m R_s}$ were calculated for each experimental temperature and the logarithms of the obtained values were fitted with polynomial functions. These functions are shown in Figs. 8 and 10 by dashed curves. Because Al atoms replace Si atoms in a random manner, and also methanols occupy different positions randomly, the activation energy for each of the three positions shows a certain distribution, centered around the mean activation energy A_0, the distribution width being σ. The pre-exponential factor is now $K_h|\omega_{bt}|$, where the frequency ω_{bt} is obtained from the Mathieu equation. Its magnitude is such that K_h varies mainly between 1 and 10. The other activation energies A_r and the pre-exponential frequencies ω_{rt} in Eq. (7) are also obtained from the Mathieu equation as the function of A_0. (They are at first calculated as the function of the potential height V_3 but presented then as the function of $A_0 = V_3 - E_0$ for numerical simulations). In the present simulations the parameter K_l was taken equal to 1. For the quadrupole frequency ν_Q of the methyl and hydroxyl groups we use 160 kHz and 205 kHz, respectively.

The simulations for Sample 2 proceed in the following way: For each position I–III we define the mean activation energy A_0, the distribution width σ and the parameter K_h. The spectral data discussed already show that the CD_3 groups of the vertical methanols II reorientate fastest and those of the horizontal methanols I slowest. Therefore, the corresponding mean activation energies are expected to behave like $A_0(I) > A_0(III) > A_0(II)$. The distribution-dependent activation energy is then $A_j = A_0 + \Delta A_j$ with ΔA_j equal to $j\sigma/20$, j = 0, ±1, ±2, … ±60. For each A_j we obtain the activation energies A_r and the frequencies ω_{rt} for the excited states (see Figs. 2 and 3), which are then used to calculate the correlation time from Eq. (7). Similarly, the tunnel frequency ω_t is obtained from $\omega_t = \omega_{0t}/(1 + \alpha T^\beta)$ by using the α and β values from Fig. 1. Then the individual relaxation rates R_{Ain} and R_{Ein} can be calculated from Eq. (4). The obtained values are compared to the limiting values L_{fm} and L_{ms} to find out the right class. The contribution to the initial relaxation rate of this class is obtained from Eq. (3), when the relative weight $w_j = \exp(-\Delta A_j^2/2\sigma^2)/\sum_j \exp(-\Delta A_j^2/2\sigma^2)$ is replaced by $(5/9)w_p w_j$ for A species and $(4/9)w_p w_j$ for E species methyl groups. The position dependent weight w_p is a parameter, which describes the occupancy of each position. Their sum has to be equal to 1. Most relaxation simulations were carried out by using equal w_p values as was done already in explaining the spectra of Sample 3. By repeating the described calculation for each j value of the three different distributions and as a function of temperature, we obtain the temperature dependence for the initial relaxation rates R_{ci} (c = f, m, s). The corresponding weights are obtained by summing up $(5/9)w_p w_j$ and $(4/9)w_p w_j$ for those rates R_{Ain} and R_{Ein}, which belong to the considered class. The results are compared with the experimental rates and weights, the parameters changed slightly and new, hopefully better initial rates calculated. The procedure was repeated so many times that the best possible agreement was reached. The simulated relaxation rates with the best-fit parameters are shown in Fig. 8 and the corresponding relative weights in Fig. 9. It is important to note that the simulations were finally

calculated simultaneously for both our samples, thus Figs. 8−9 include also the effect of the hydroxyl deuterons on the fit. The total number of parameters for Sample 2 (NaY with 200 % CD_3OH) is 9 (when all three $w_p(i)$'s were assumed equal) consisting of the three sets of A_0, σ and K_h.

4.2. Sample 3

In the first simulations for sample 3 (containing 200 % of CD_3OD) we kept the mentioned 9 parameters constant and concentrated to find out suitable parameters to describe the motion of OD deuterons in the three positions. To determine the parameters q and T_{lj} in the efficiency factor $E = q \exp(-T_{lj}/T)$ for the OD's in position I (section 2.2.), we required that (i) E has to decrease by the factor 10 between the temperatures 60 K and 20 K similarly to the experimental relaxation rate of the intermediate component and (ii) the effective quadrupole frequency, equal to $(1/2)(3\cos^2\Delta - 1)\nu_Q$, has to be practically equal to $\nu_Q = 205$ kHz at 20 K and to 150 kHz at 60 K according to the experimental spectra. This leads to q = 1.694 and $T_{lj} = 70.64$ K. To guarantee that the OD(I) reorientation contributes significantly to the deuteron relaxation for $T > 80$ K, we defined the temperature T_E, above which the efficiency factor 1 – E remains constant. In simulations $T_E = 87$ K was the optimum choice.

Thus we have introduced one set of motional parameters for the rotation of hydroxyls I and III above 80 K, which means 3 parameters. In addition, there are 7 more parameters describing the distribution of the correlation time of the limited jumps of hydroxyls I and III**,** the distribution of the relaxation rate of hydroxyls II**,** and the temperature T_E related to the efficiency factor E**.** These parameters describe temperature–independent behaviours and were not varied in the simulations. Thus the total number of real motional parameters for Samples 1 and 3 is 12. This is a large number, but also the number of independent results is large, altogether 10 curves, describing partly the temperature dependence of the relaxation rates (6 curves) and of the relative weights (4 curves, since the sum of relative weights equals 1). So on average there is clearly less than two parameters per curve. Two parameters per curve is the common case when the temperature dependence of an exponential relaxation rate is explained by the Arrhenius equation, which depends on two parameters.

Simulations for Sample 3 are carried out similarly to those for Sample 2, only the weights have to be modified because there are now four deuterons in a methanol molecule. For A and E species methyl groups the weight w_j in (3) has to be replaced by $(5/12)w_pw_j$ and $(4/12)w_pw_j$, respectively, while for the hydroxyl deuteron the corrected weight is $(1/4)\ w_pw_j$. At first the methyl parameters were kept constant and best-fit values for the hydroxyl parameters were searched. When the best fit was obtained, we varied mainly the parameters for methyl groups and hydroxyls in positions I (and III) to find out how much individual parameters can be varied without appreciable changes in the overall fit. Also different w_p values were tried. Best fits were as good as those in Figs. 8–11 but were not considered possible because the spectra seem to require equal w_p values. The best fit by eye, based on equal w_p values, was obtained with the parameters given in Table II and is shown in Figs. 10–11 by continuous curves. These parameters constitute the main result of our relaxation simulations.

Let us consider in more detail the small maximum in the experimentally observed rate of the fast relaxing component of Sample 3 near 100 K (Fig. 10). For Sample 2 the corresponding rate (no maximum in it) is clearly larger than for Sample 3. Therefore, the hydroxyl deuterons of Sample 3 have an important role. Because they relax rather

slowly, the limiting values L_{fm} and L_{ms} for this sample are clearly smaller than for Sample 2. Consequently, some methyl deuterons, which in Sample 2 contribute to the intermediate component, contribute to the fast component in Sample 3. Therefore, the fast-component relaxation rate of samples 2 and 3 differ from each other although they are both related, almost exclusively, to the methyl deuterons. The hydroxyl deuterons contribute to the intermediate and slow components according to our simulations.

5. Discussion

The main aim of the present study was to improve the recently presented method for describing the deuteron relaxation in the presence of wide activation energy distributions [16]. We introduced two features, the temperature dependent tunnel splitting and a special temperature dependence for the correlation time of the methyl motion, not describable by a constant activation energy. Both these new features were derived from the Mathieu equation by using somewhat semiquantitative although well established methods. They modify the theoretically calculated rates and weights at lowest temperatures. The inclusion of the tunnel frequency ω_t in the relaxation rates of Eqs. (4) tends to increase the rate and weight of the fast relaxing component. This causes a small shift of the corresponding mean activation energy towards larger values. Best fits to experimental data were obtained with such distributions, for which ω_t can be equal to ω_0 only at the low-energy wing of the distribution. The use of Eq. (7) for the methyl correlation time shortens it at low temperatures. This decreases the weight of the slow component and increases its relaxation rate, leading to a better agreement with experiment. Furthermore, nearly all the calculated relaxation rates are in the experimentally observed range (that is the considered deuterons relax faster than the longest waiting time). The combined effect of these two improvements is demonstrated in Figs. 9 and 11 by the calculated weights of the three components. The continuous curves take into account both these improvements, while the dashed curves exclude them. Above 40 K the curves practically agree with each other but deviate increasingly at lower temperatures. We took into account even those deuterons for which the calculation gives relaxation rates slower than the rate of the slow component. Their number is practically negligible when the improvements are taken into account but quite large when the improvements are excluded. The former curves agree clearly better with the experimental results especially for Sample 3.

In general the agreement between the experimental values and simulated curves is reasonable and also consistent with the temperature dependence of spectral components. The biggest deviation is found in the calculated relaxation rate of the intermediate component, which exceeds the observed value. Of course a part (though not all) of the deviation is related to the fact that the experimental relaxation rates for each of the three components are average rates trying to describe the nonexponential relaxation of a certain component with one exponential, while the calculated rates represent the initial rates. Therefore, the calculated rates can be somewhat larger than the observed rates. This difference should not be important as far as the main interest is in the temperature dependence of the rates and weights, not so much in single values for fixed temperatures. Naturally, the use of average relaxation rates instead of initial ones could be one improvement in future simulations, but the most difficult problem presently is the very vague knowledge of the motion of the hydroxyl deuterons.

There are also other features which might improve the present model if they could be taken properly into account. One could use four exponentials to describe the experimentally observed signal recovery, if the individual relaxation rates span four or more orders of magnitude. Of course this would require very accurate experiments with very little scatter. As described in Introduction, the choice of using three exponentials instead of four or five is a consequence of the limited experimental accuracy, it does not derive from any theoretical reasons. Another point is the coupling of the tunnelling reservoir to the relaxation of the magnetizations M_A and M_E, which may have some effect when the tunnel and resonance frequencies are practically equal. In the present study this was taken into account only qualitatively, which was considered sufficient because the relevant activation energy distributions extend only very marginally to values consistent with $\omega_t > \omega_0$. Still another possibility is the different coherence damping rates k_K and k_t. Their effect on the relaxation rates of the magnetisations M_A and M_E was already calculated and presented in Supplemental Material, but their introduction to simulations would introduce additional parameters for each methanol position I–III.

Acknowledgements

We thank Dr Grzegorz Stoch for participation in some measurements and Dr Kinga Góra-Marek for preparation of samples. Financial support from Jenny and Antti Wihuri Foundation is acknowledged. This study was a part of the project generously financed by the National Science Centre, Poland, grant No. N202 127939 during 2010 - 2014.

References

[1] J.S. Blicharski, Z.T. Lalowicz, W. Sobol, J. Phys. C: Solid State Phys. 11 (1978)4187–4200.
[2] Z.T. Lalowicz, W.T. Sobol, J. Phys. C: Solid State Phys. 16 (1983) 2351–2362.
[3] Z.T. Lalowicz, U. Werner, W. Müller-Warmuth, Z. Naturforsch. 43a (1988) 219–227.
[4] A. Detken, P. Focke, H. Zimmermann, U. Haeberlen, Z. Olejniczak, Z.T. Lalowicz, Z. Naturforsch. 50a (1995) 95–116.
[5] J.C. Pratt, A. Watton, J. Phys. C: Solid State Phys. 19 (1986) 5729–5744.
[6] D. van der Putten, N.J. Trappeniers, Physica A 129 (1985) 302–326.
[7] L.P. Ingman, E. Koivula, Z.T. Lalowicz, M. Punkkinen, E.E. Ylinen, Z. Phys. B – Condensed Matter 66 (1987) 363–373.
[8] L.P. Ingman, E. Koivula, Z.T. Lalowicz, M. Punkkinen, E.E. Ylinen, J. Chem. Phys. 88 (1988) 58–67.
[9] L.P. Ingman, E. Koivula, M. Punkkinen, E.E. Ylinen, Z.T. Lalowicz, Physica B 162 (1990) 281–292.
[10] G. Diezemann, H. Sillescu, D. van der Putten, Z. Phys. B – Condensed Matter 83 (1991) 245−257.
[11] G. Diezemann, Appl. Magn. Reson. 17(1999) 345–366.
[12] E. Rössler, M. Taupitz, K. Börner, M. Schulz, H.-M. Vieth, J. Chem. Phys. 92 (1990) 5847–5855.

[13] P.M. Cereghetti, R. Kind, J.S. Higgins, J. Chem. Phys. 121 (2004) 8068–8078.
[14] J.M. Griffin, A.J. Miller, A.J. Berry, S. Wimperis, S.E. Ashbrook, Phys. Chem. Chem. Phys. 12 (2010) 2989–2998.
[15] Z.T. Lalowicz, G. Stoch, A. Birczyński, M. Punkkinen, E.E. Ylinen, M. Krzystyniak, K. Góra-Marek, J. Datka, Solid State Nucl. Magn. Reson. 45–46 (2012) 66–74.
[16] G. Stoch, E.E. Ylinen, A. Birczyński, Z.T. Lalowicz, K. Góra-Marek, M. Punkkinen, Solid State Nucl. Magn. Reson. 49−50 (2013) 33–41.
[17] J.C. Pratt, A. Watton, H.E. Petch, J. Chem. Phys. 73 (1980) 2542–2546.
[18] M. Prager, A. Heidemann, Chem. Rev. 97 (1997) 2933–2966.
[19] J. Haupt, Z. Naturforsch. 26a (1971) 1578–1589.
[20] W. Müller-Warmuth, R. Schüler, M. Prager, A. Kollmar, J. Chem. Phys. 69 (1978) 2382–2392.
[21] J.L. Skinner, H.P. Trommsdorff, J. Chem. Phys. 89 (1999) 345–366.
[22] E.O. Stejskal, H.S. Gutowsky, J. Chem. Phys. 28 (1955) 388–396.
[23] S. Clough, A. Heidemann, A.J. Horsewill, J.D. Lewis, N.J. Paley, J. Phys. C: Solid State Phys. 15 (1982) 2495–2508.
[24] S. Szymanski, J. Chem. Phys. 111 (1999) 288–299.
[25] P. Gutsche, H. Schmit, U. Haeberlen, T. Ratajczyk, S. Szymanski, ChemPhysChem 7 (2006) 886–893.
[26] M. Kankaanpää, M. Punkkinen, E.E. Ylinen, Mol. Phys. 100 (2002) 2877–2893.
[27] M.W. Anderson, P.J. Barrie, J. Klinowski, J. Phys. Chem. 95 (1991) 235–239.
[28] J. Hunger, I.A. Beta, H. Böhling, C, Ling, H. Jobic, B. Hunger, J. Phys. Chem. B110 (2006) 342−353.
[29] C. Beauvais, X. Guerrault, F.-X. Coudert, A. Boutin, A.H. Fuchs, J. Phys. Chem. B 108 (2004) 399−404.
[30] M. Hunger, U. Schenk, A. Buchholz, J. Phys. Chem. B 104 (2000) 12230−12236.
[31] L. Zhu, K. Seff, D.H. Olson, B.J. Cohen, R.B. Von Dreele, J. Phys. Chem. B 103 (1999) 10365−10372.
[32] K. Góra-Marek, Vibr. Spectrosc. 52 (2010) 31−38.
[33] A. Birczyński, M. Punkkinen, A.M. Szymocha, Z.T. Lalowicz, J. Chem. Phys. 127 (2007) 204714, 1−10.
[34] G.C. Lickfield, A.L. Beyerlein, G.B. Savitsky, L.E. Lewis, J. Phys. Chem. 88 (1984) 3566−3570.
[35] A.M. Szymocha, A. Birczyński, Z.T. Lalowicz, G. Stoch, M. Krzystyniak, K. Góra-Marek, J. Phys. Chem. A 118 (2014) 5359−5370.
[36] Z.T. Lalowicz, G. Stoch, A. Birczyński, M. Punkkinen, M. Krzystyniak, K. Góra-Marek, J. Datka, Solid State Nucl. Magn. Reson. 37 (2010) 91−100.
[37] G. Diezemann, J. Phys.: Condens. Matter 4 (1992) 9153–9180.
[38] M. Kankaanpää, E.E. Ylinen, M. Punkkinen, Solid State Nucl. Magn. Reson. 23 (2003) 224–242.

Table I
Contribution of methyl and hydroxyl deuterons of methanol molecules in positions I, II and III to respective spectral components for Sample 3

Spectral components	160 K		100 K	90K ÷ 60 K		25 ÷ 20K
Rotation CD_3 ν_Q = 150 kHz	CD_3 I +CD_3 III 50 % (50 %)	↓	CD_3 I + CD_3 III + OD III 62 % (58.3 %)	CD_3 I + OD I + CD_3 III + OD III 68 % (66.7 %)	↑	CD_3 III 24 % (25 %)
Tunnelling CD_3 ν_Q = 150 kHz					↓	1/2 CD_3 II 14 % (12.5 %)
Rotation OD ν_Q = 120 kHz	OD I + OD III 18 % (16.7 %)	↑	OD I 6 % (8.3 %)			
Gauss	CD_3 II 23 % (25 %)	constant	CD_3 II 23 % (25 %)	CD_3 II 23 % (25 %)	↑	1/2 CD_3 II +1/2 OD III 17 % (16.7 %)
Rigid	OD II 9 % (8.3 %)	constant	OD II 9 % (8.3 %)	OD II 9 % (8.3 %)	↓	OD I + OD II + 1/2 OD III + CD_3 I 45 % (45.8 %)

Table II
Motional parameters for methyl and hydroxyl groups of methanols in NaY(2.4)

	CD_3(I)	CD_3(II)	CD_3(III)	OD(I, III)(rot)
A_0 (kJ/mol)	5.3	4.2	4.6	8.0
σ (kJ/mol)	1.7	0.9	0.7	0.8
τ_0 (10^{-14} s)				0.2
K_h	2.0	2.0	2.0	

Figure captions

FIG. 1. The calculated values for the parameters α (open circles) and β (filled circles) as the function of the activation energy A_0, together with the fitting curves. The vertical scales for α (right) and β (left) are different.

FIG. 2. The excited-state activation energies $A_r = E_r - E_0$ and A_0 (straight line) as the function of A_0. The curve below the horizontal axis describes $-E_0$.

FIG. 3. The tunnel frequencies $|\nu_{rt}|$ and $|\nu_{bt}|$ as the function of A_0.

FIG. 4. Representative positions of methanol molecules at a segment of NaY(2.4) supercage wall. The methanol at position I (called horizontal) is bonded to the sodium cation SII, at position II (called vertical) is hydrogen−bonded to a framework oxygen, and at position III is hydrogen−bonded to the hydroxyl deuteron of the methanol at position I (representing a second adsorption layer or the first molecule of a possible chain).

FIG. 5. The deuteron spectra of Samples 1 (100 % of CD_3OH) at 5 K (a) and 2 (200 % of CD_3OH) at 10 K (b). Contributions of the rotating (i) and tunnelling (ii) methyl groups, as well as of rigid (Pake doublet) and Gaussian spectral components are shown separately.

FIG. 6. The deuteron spectrum of Sample 3 (200 % of CD_3OD) at different temperatures.

FIG. 7. The relative contributions of various spectral components of Sample 3 as the function of temperature.

FIG. 8. The observed relaxation rates R_f, R_m and R_s as the function of temperature for Sample 2 (200 % of CD_3OH). The continuous curves represent the best-fit simulated results. The dashed curves describe the limiting values L_{fm} and L_{ms}.

FIG. 9. The experimental weights of the fast, intermediate and slow components of Sample 2 (200 % of CD_3OH), together with the simulated weights (continuous curves). The dashed curves show the simulated weights when $\omega_t = 0$ and the effect of the excited rotational levels on the correlation time [Eq. (7)] was excluded.

FIG. 10. The same as Fig. 8 but for Sample 3 (200 % of CD_3OD).

FIG. 11. The same as Fig. 9 but for Sample 3 (200 % of CD_3OD).

highlights

Non-exponential deuteron spin−lattice relaxation and activation energy distributions

- The effect of a large tunnel splitting and decreasing activation energy on relaxation
- Simulation of temperature-dependent relaxation rates
- Application to zeolite NaY(2.4) containing methanol molecules
- Interpretation of deuteron spectra

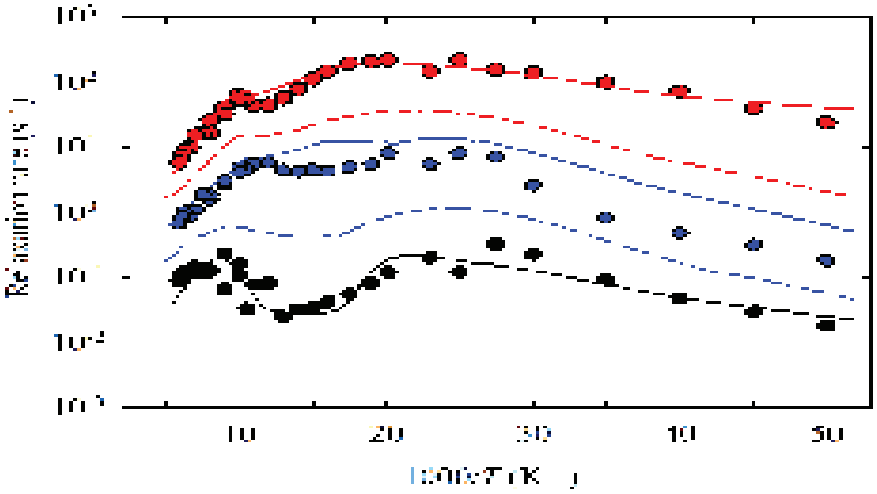

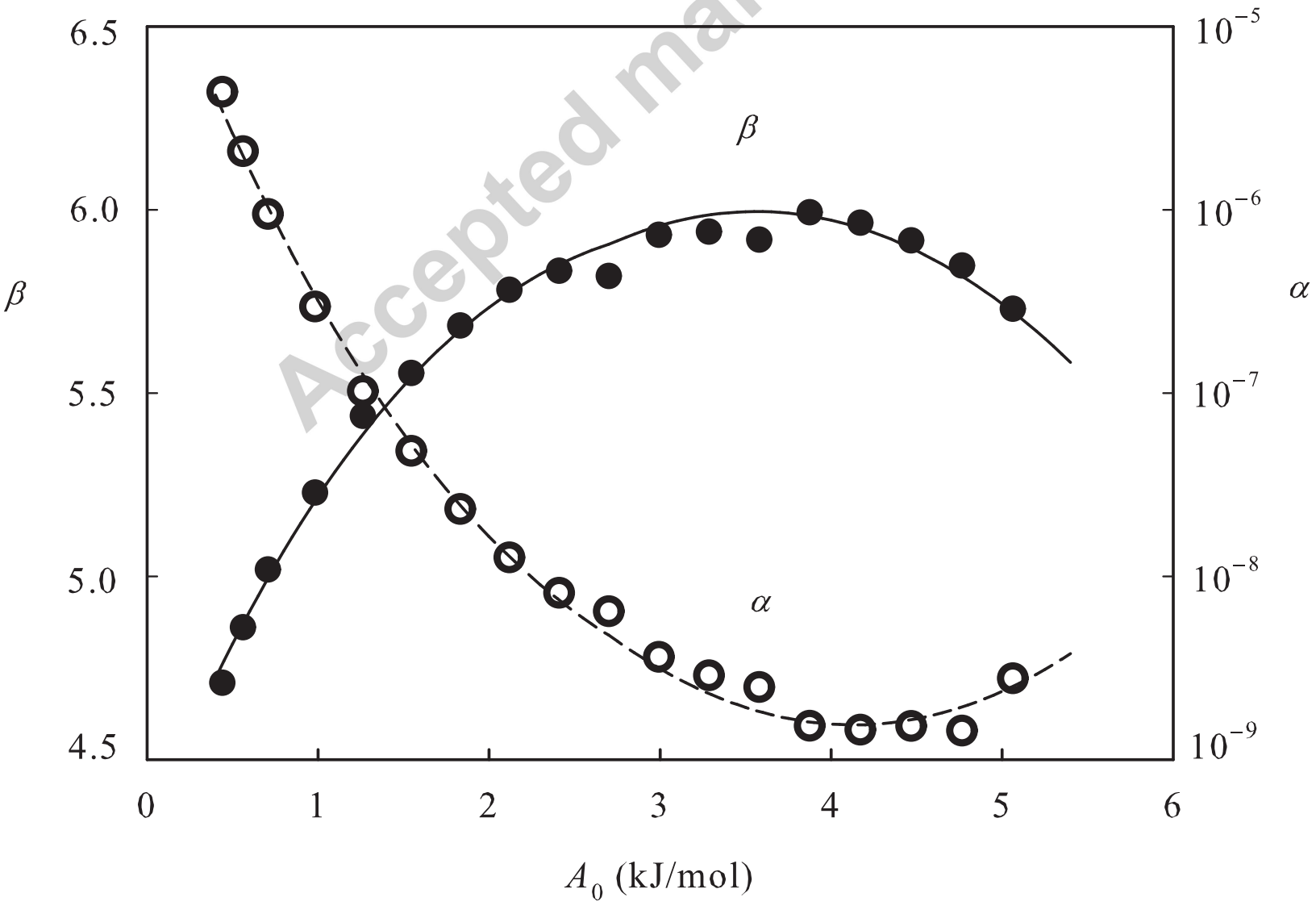

Figure 2

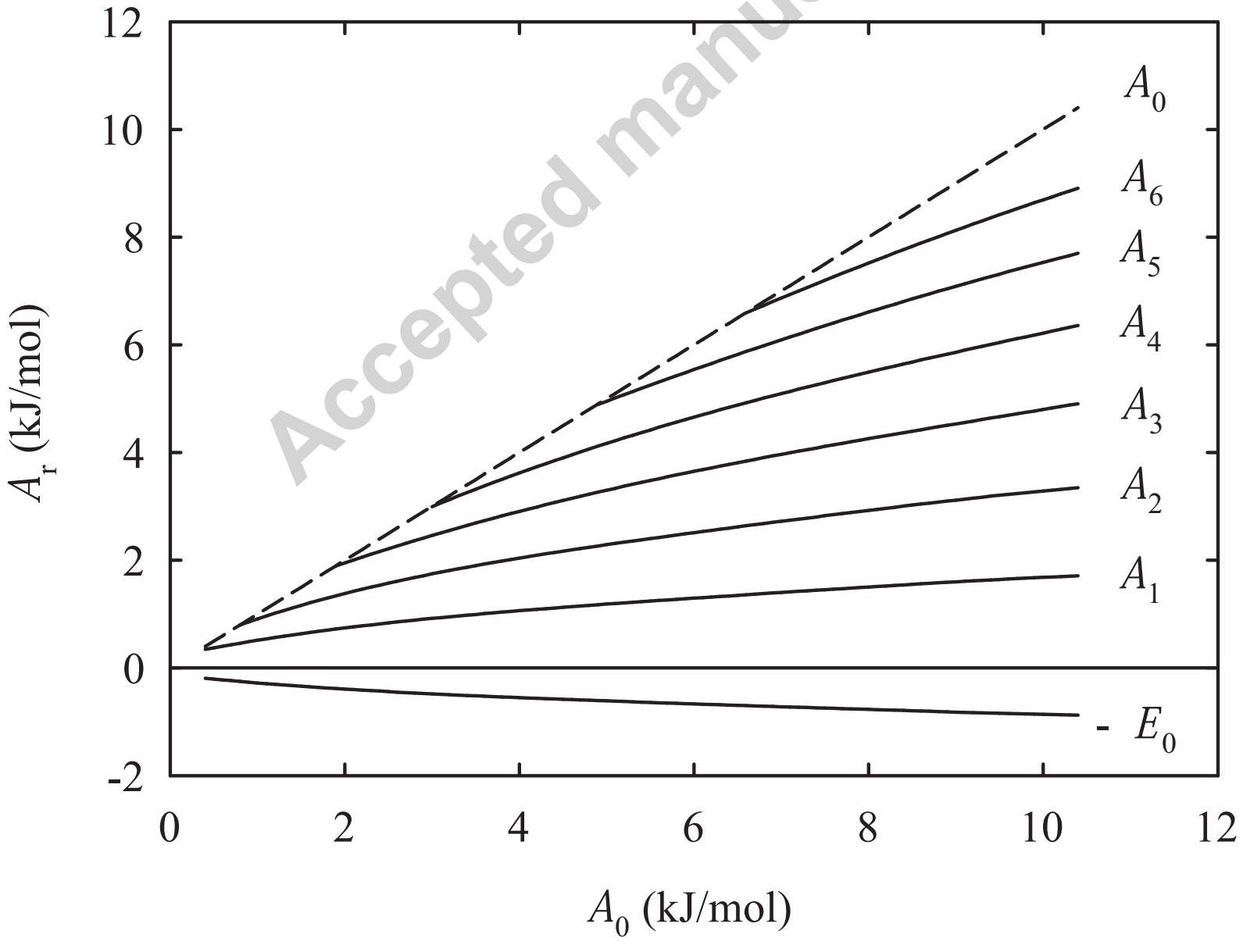

Figure 3

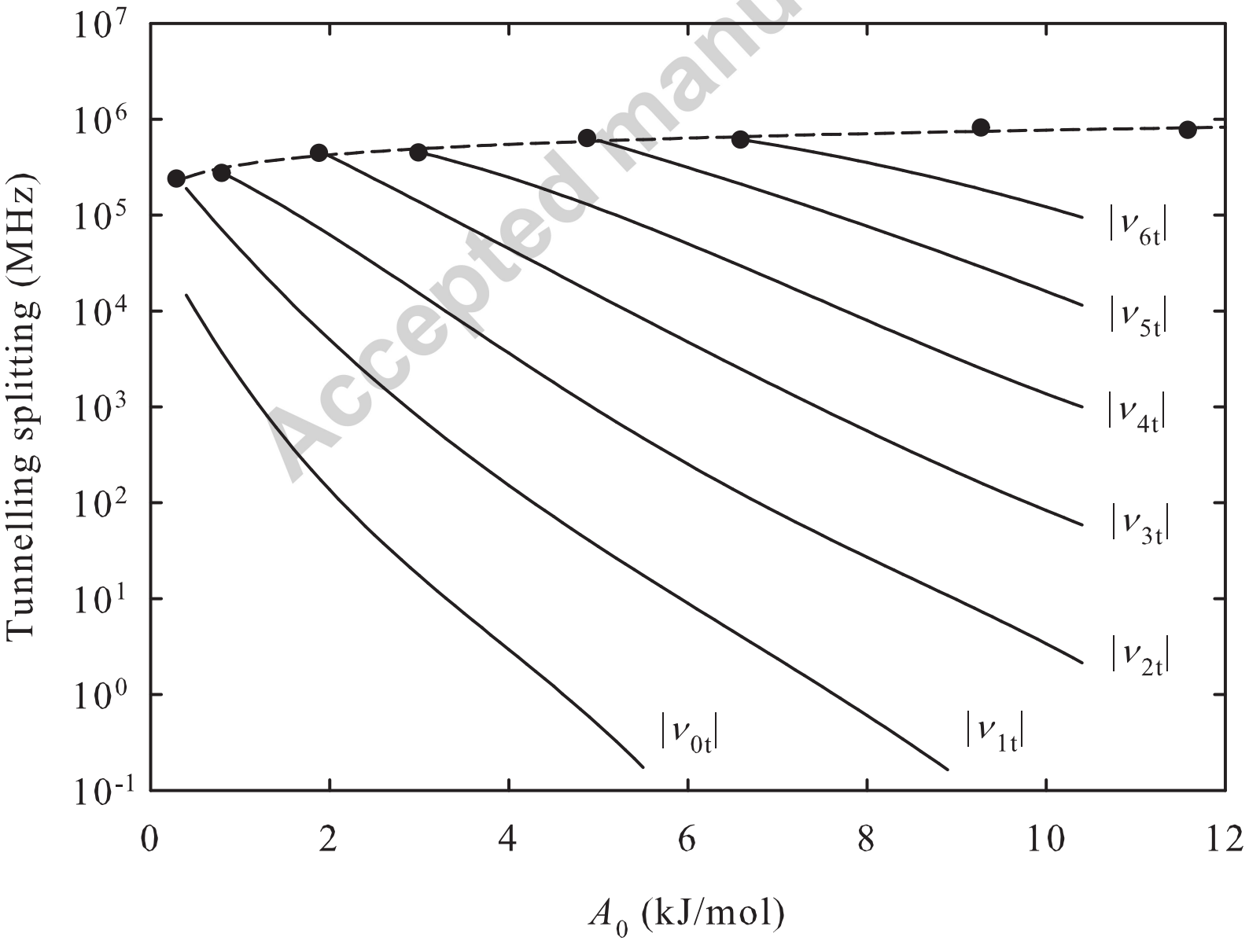

Figure 4

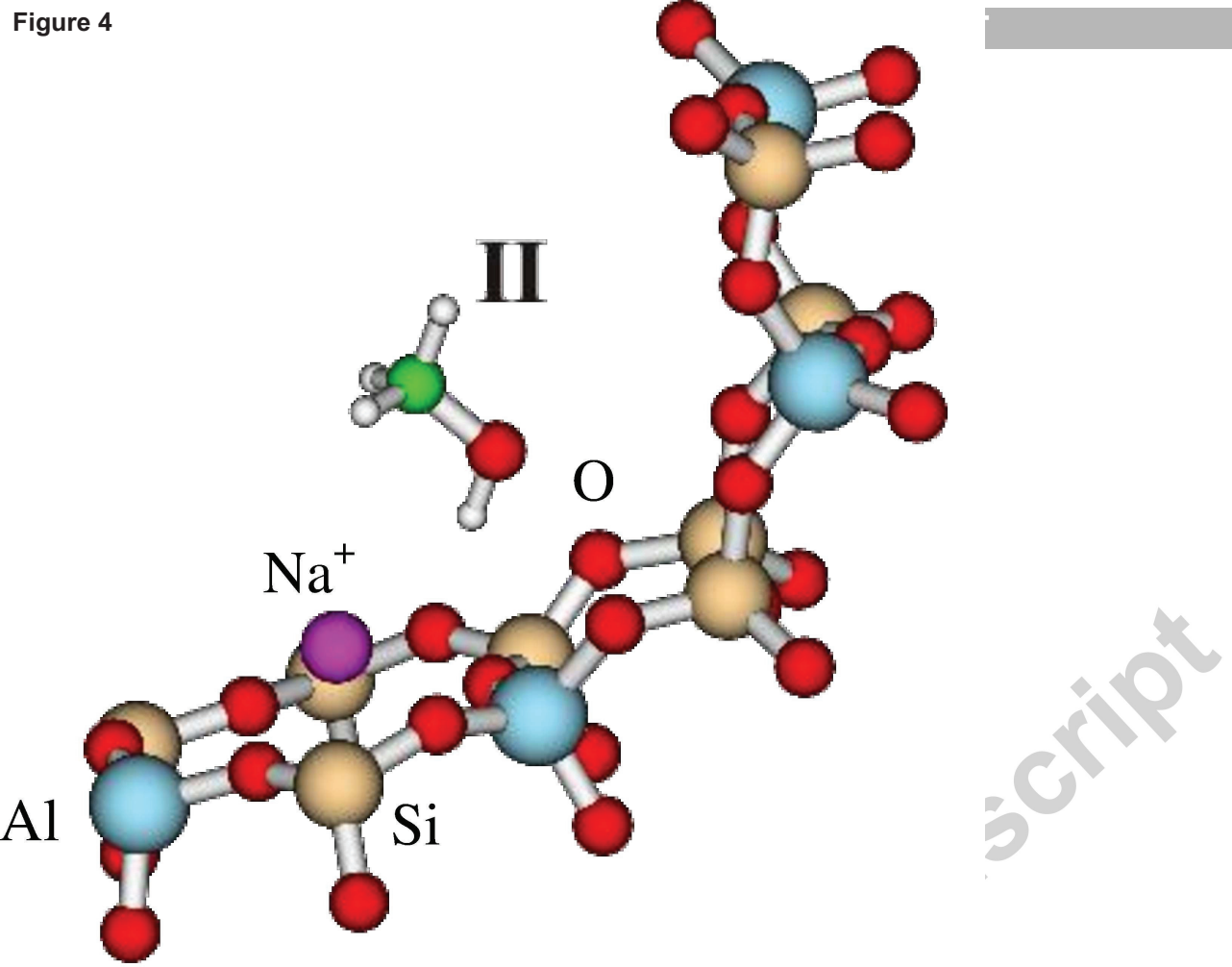

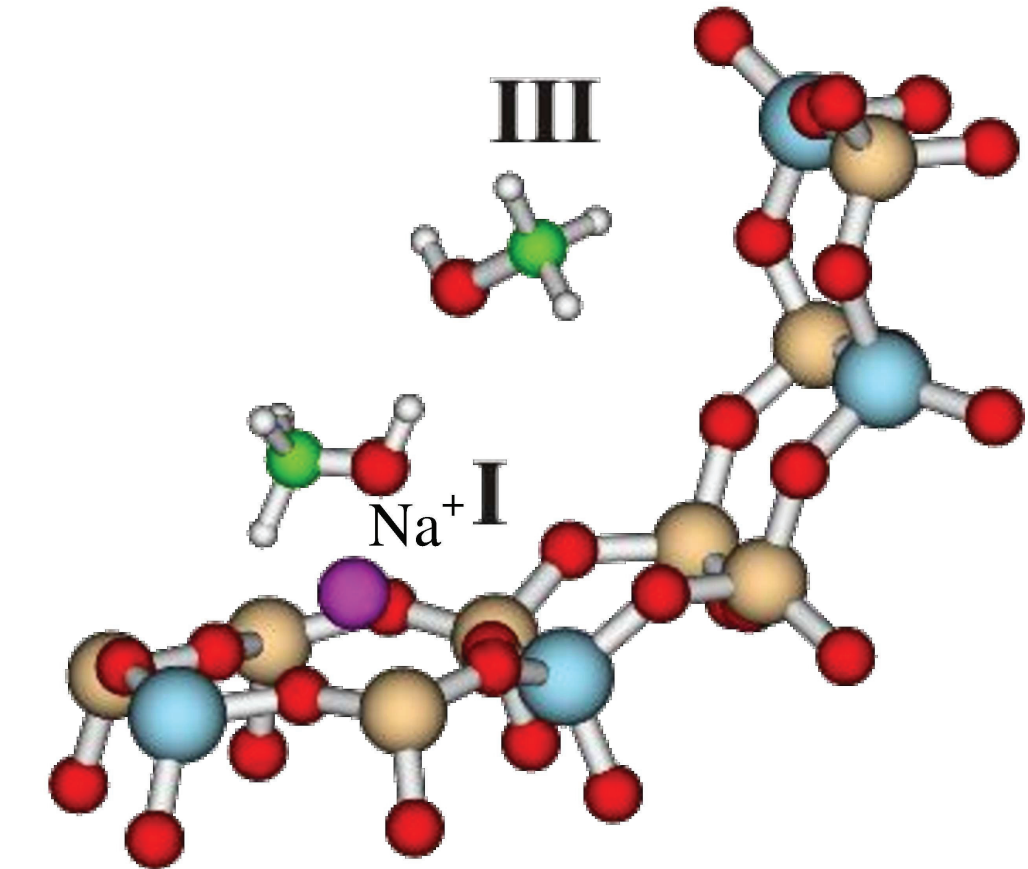

Figure 5

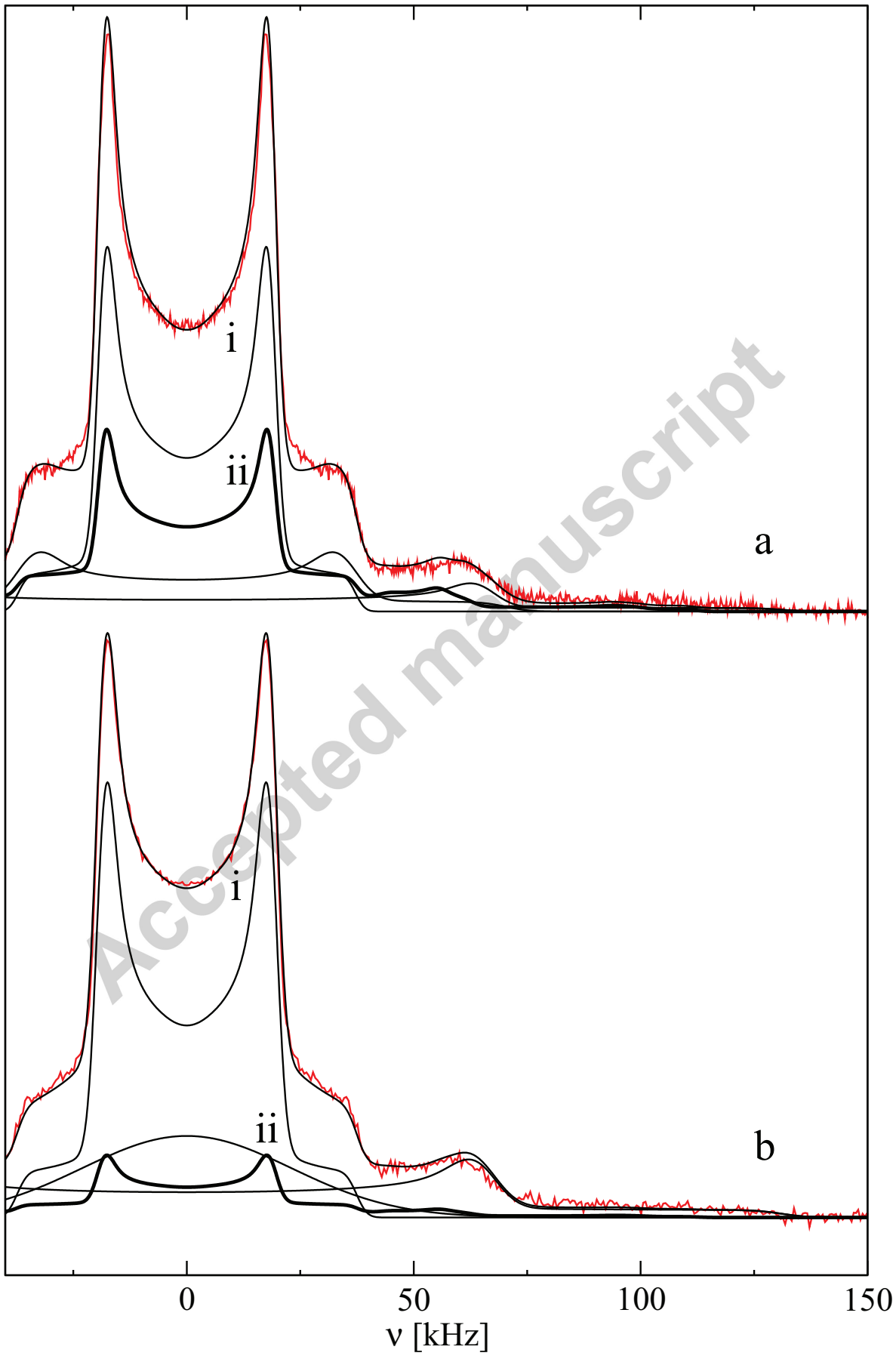

Figure 6

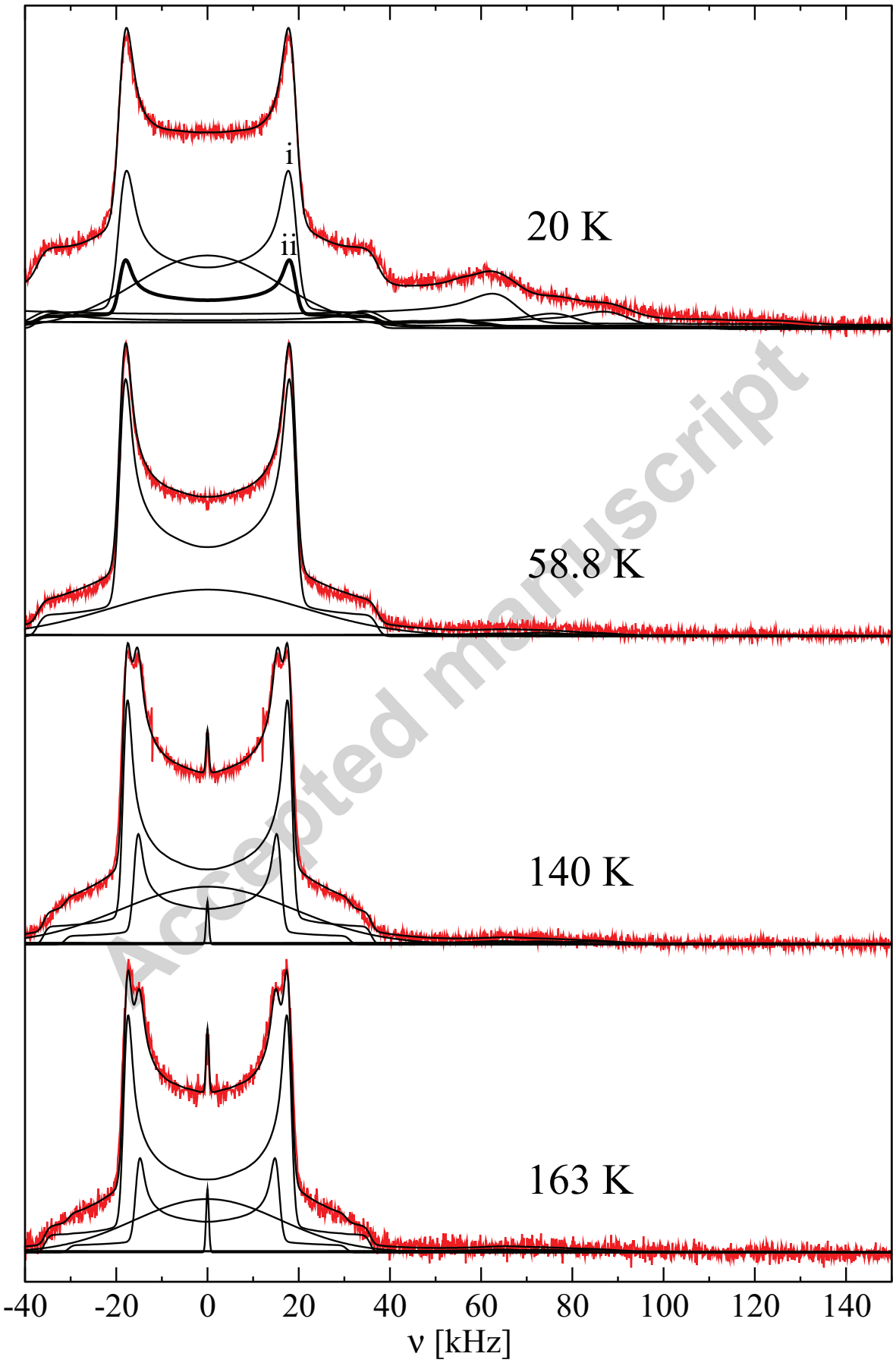

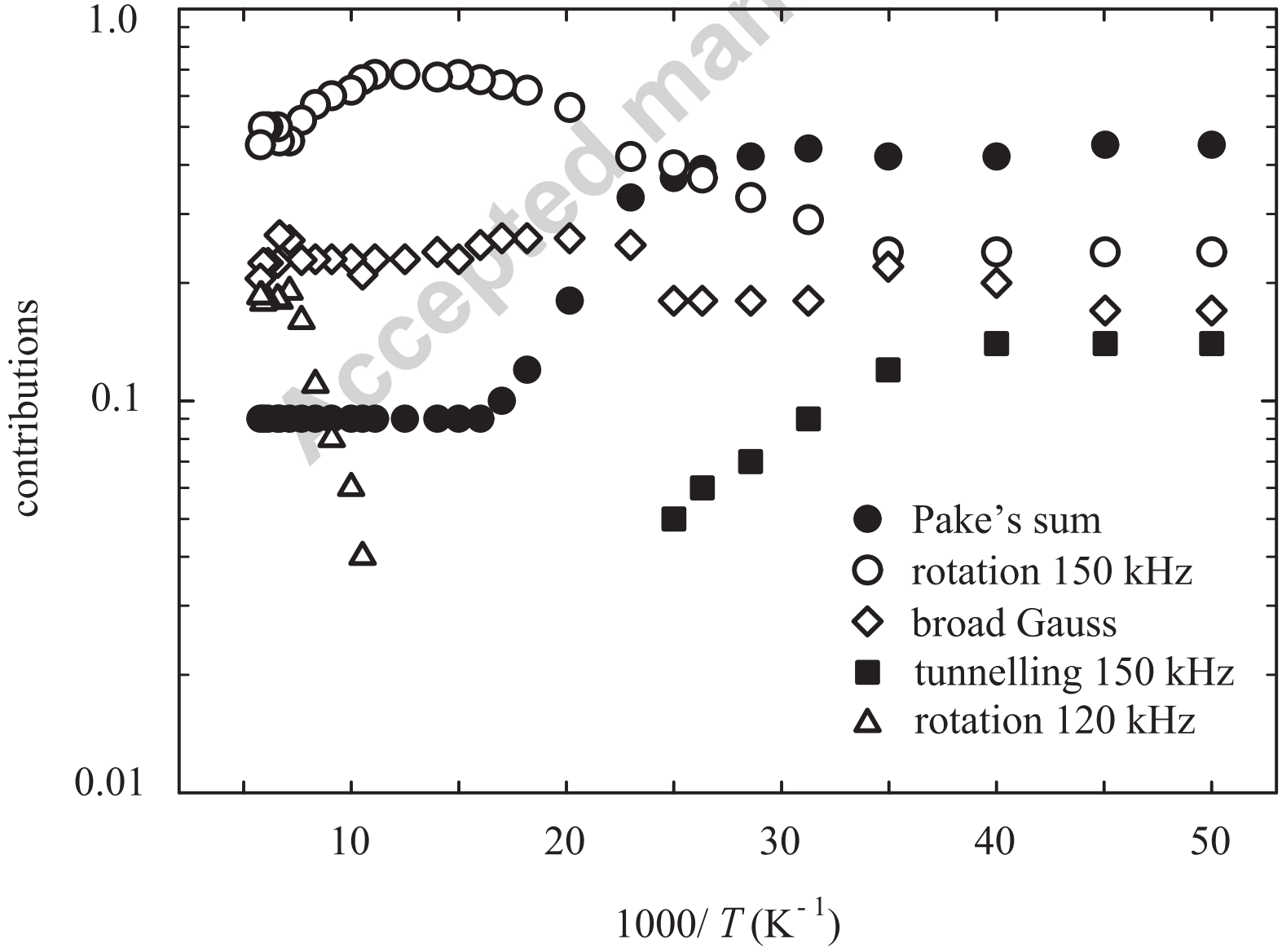

Figure 8

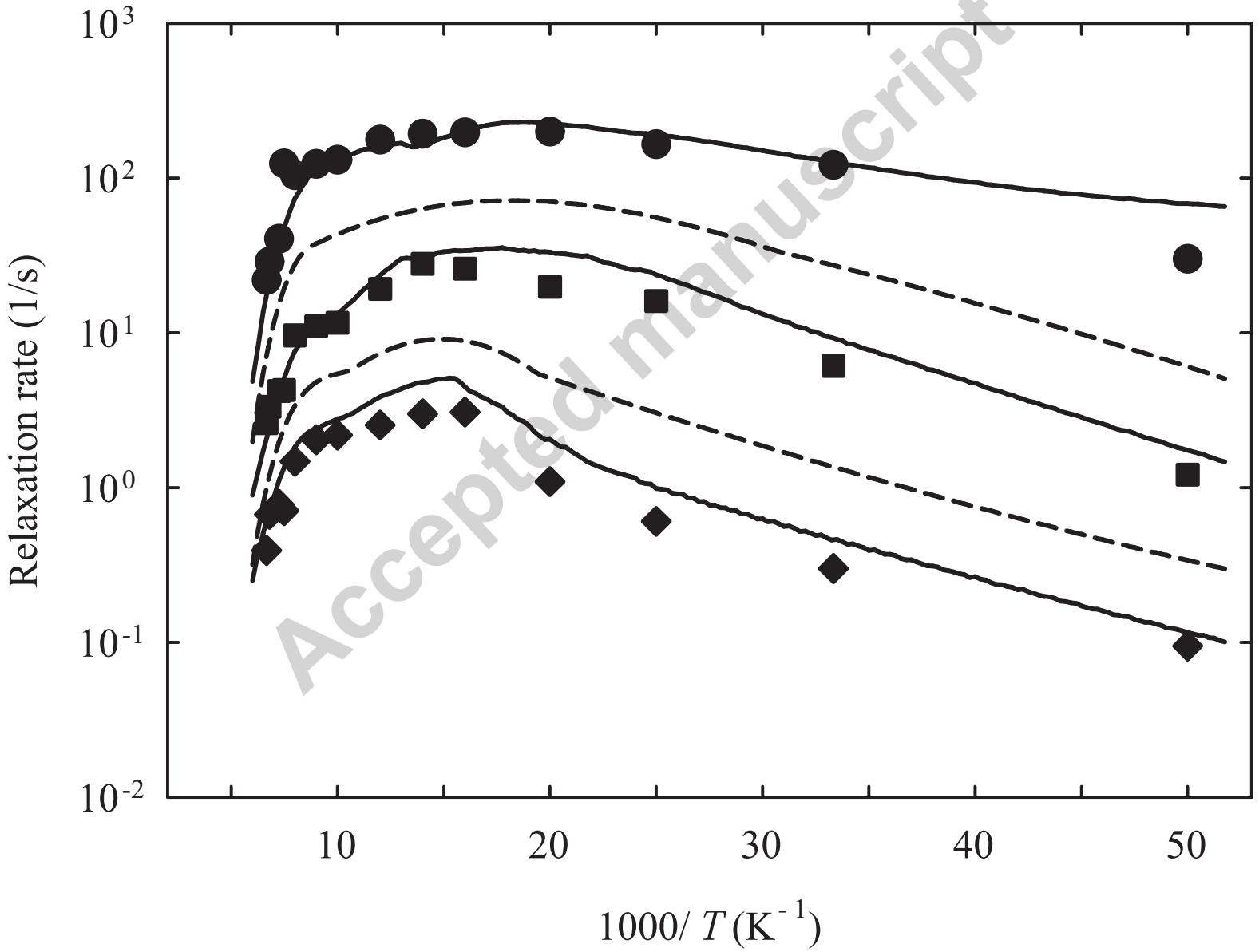

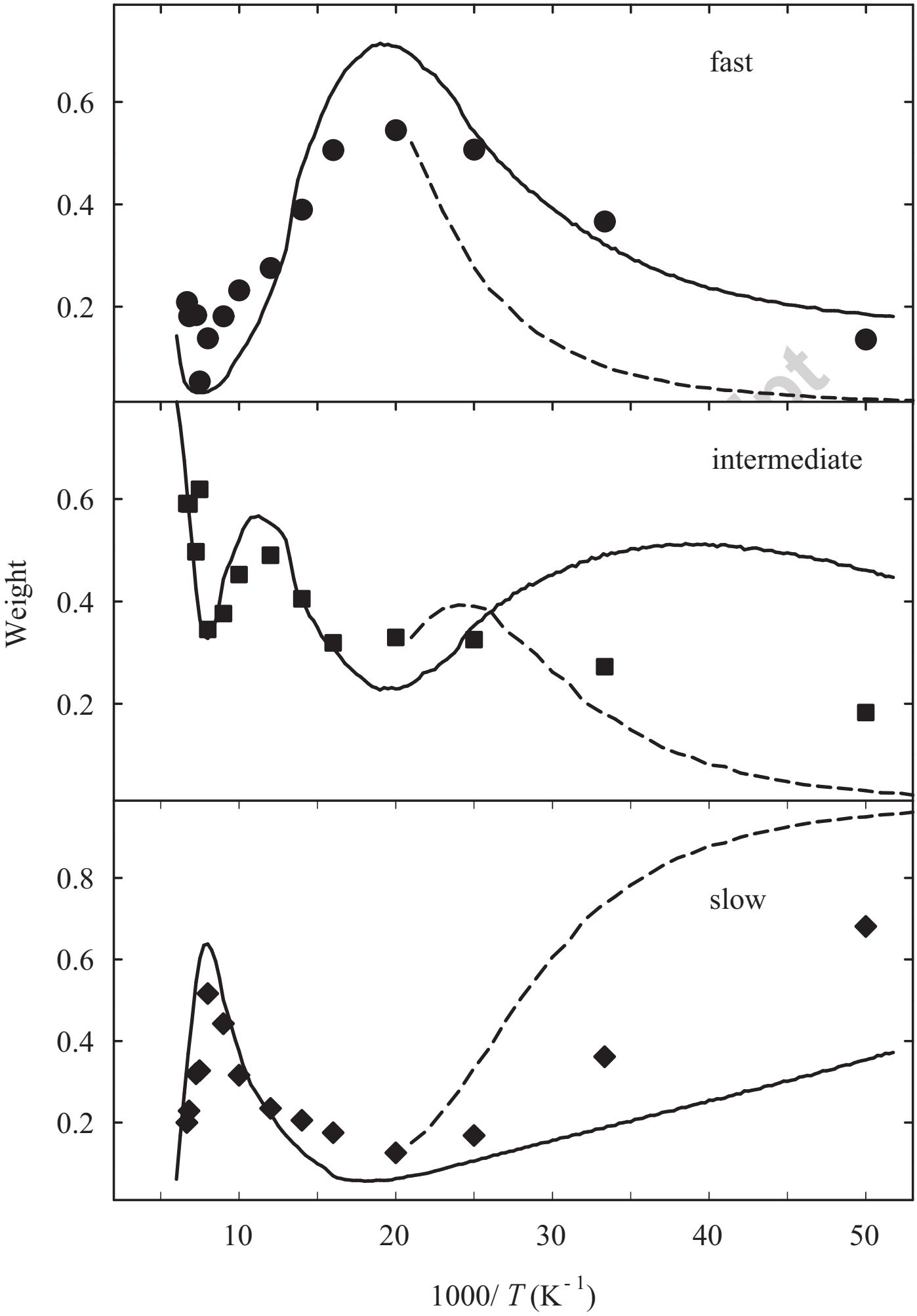

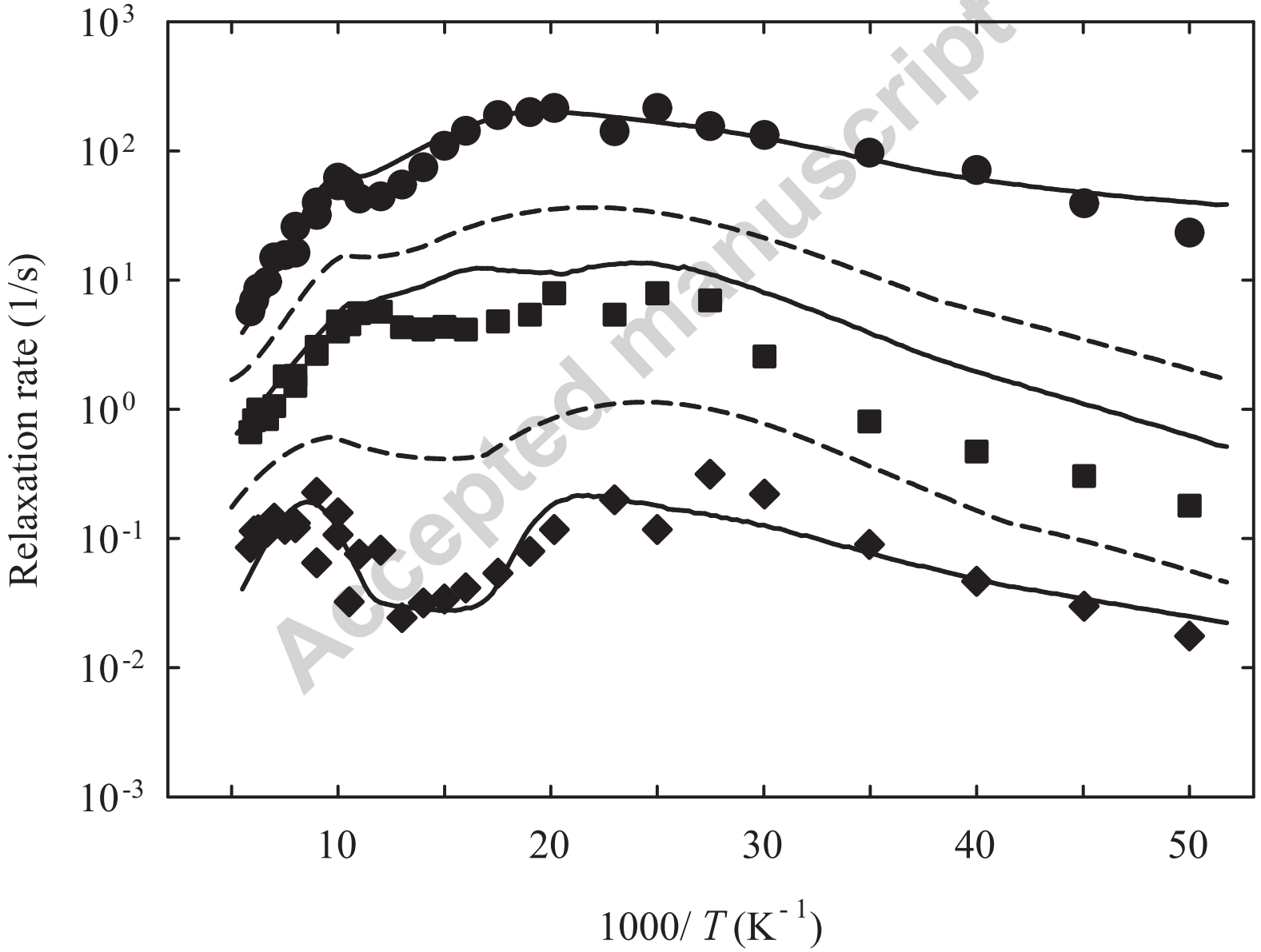

Figure 11

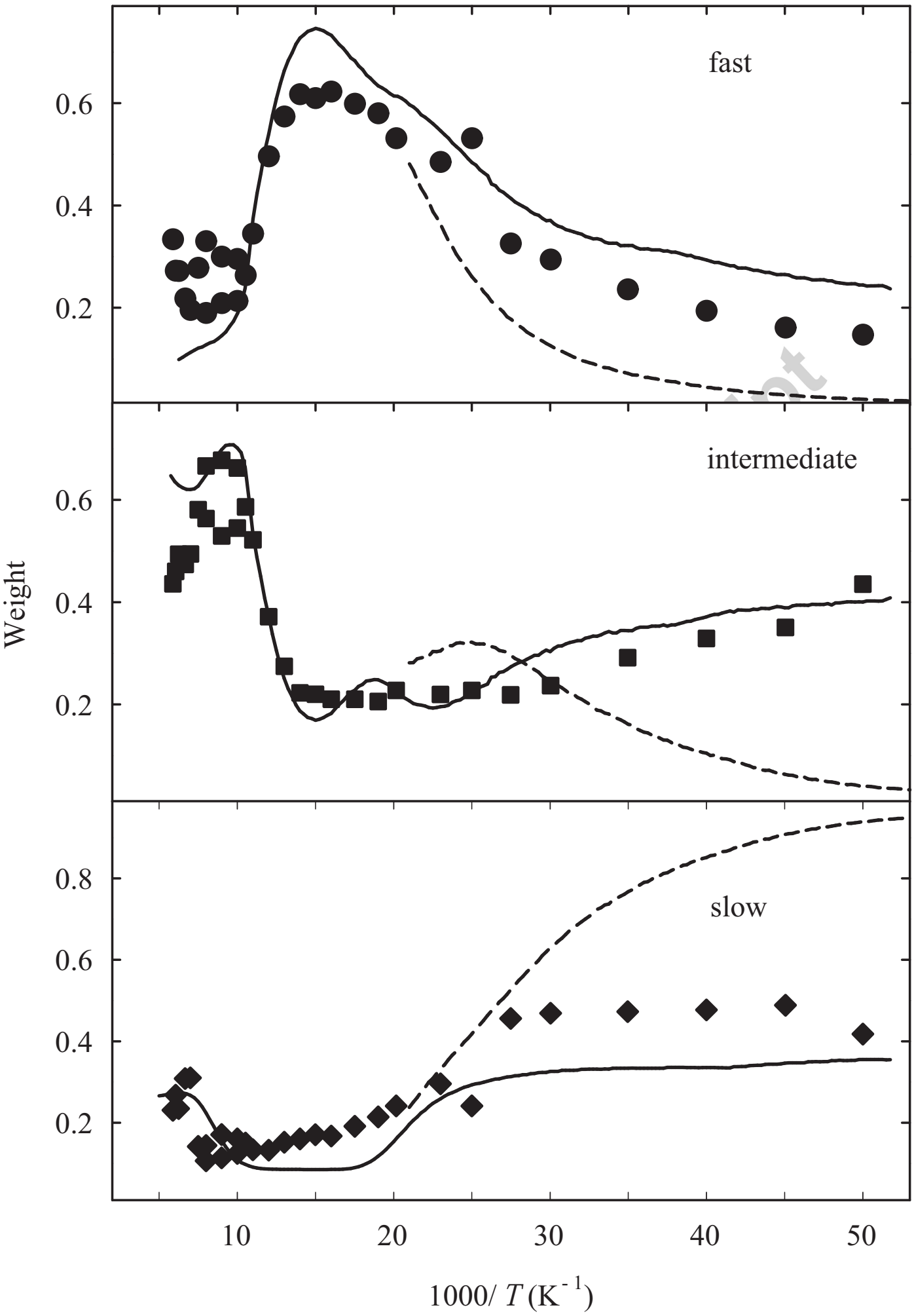

Supplementary Material to the article:

The effect of a broad activation energy distribution on deuteron spin–lattice relaxation

E.E. Ylinen, M. Punkkinen, A. Birczyński, Z.T. Lalowicz

Deuteron spin–lattice relaxation in CD_3 containing compounds with a large tunnel splitting

S1. Spin and rotational functions

There are some theoretical models for deuteron relaxation in CD_3 compounds when the tunnelling frequency ω_t is much smaller than the deuteron resonance frequency ω_0 [5, 17] and also two which should be valid in the case of large tunnelling frequencies $\omega_t >> \omega_0$ [10, 11]. Ref. 10 discusses the relaxation of the deuteron magnetization $Mz = M_A + M_E$ without any coupling to other relatively slowly relaxing quantities, for example the tunnelling reservoir. The work [11] considers also these couplings. Unfortunately, neither of them takes into account the fact that the magnetizations M_A and M_E can relax at different rates, especially in the slow-motion regime for $\omega_t >> \omega_0$. Because this fact is crucially important for the present study, we derive the required expressions in detail below by using an approach somewhat different from [10, 11].

The three deuterons are denoted by u, v and w. Their spin quantum numbers m are defined by a row symbol, for example (10–1) means that the m values of these deuterons are 1, 0 and –1, respectively. In the derivation we use the symmetrised spin functions

$$
\begin{aligned}
&S_{A3} = (111)\\
&S_{A2} = (1/\sqrt{3})[(110) + (011) + (101)]\\
&S_{A1} = (1/\sqrt{3})[(11\text{–}1) + (\text{–}111) + (1\text{–}11)]\\
&S'_{A1} = (1/\sqrt{3})[(001) + (100) + (010)]\\
&S_{A0} = (1/\sqrt{6})[(1\text{–}10) + (\text{–}110) + (01\text{–}1) + (0\text{–}11) + (\text{–}101) + (10\text{–}1)]\\
&S'_{A0} = (1/\sqrt{6})[(1\text{–}10) - (\text{–}110) + (01\text{–}1) - (0\text{–}11) + (\text{–}101) - (10\text{–}1)]\\
&S''_{A0} = (000)\\
&S_{Ea2} = (1/\sqrt{3})[(110) + \varepsilon(011) + \varepsilon^*(101)]\\
&S_{Ea1} = (1/\sqrt{3})[(11\text{–}1) + \varepsilon(\text{–}111) + \varepsilon^*(1\text{–}11)] \qquad \text{(S1)}\\
&S'_{Ea1} = (1/\sqrt{3})[(001) + \varepsilon(100) + \varepsilon^*(010)]\\
&S_{Ea0} = (1/\sqrt{6})\{(1\text{–}10) + (\text{–}110) + \varepsilon[(01\text{–}1) + (0\text{–}11)] + \varepsilon^*[(\text{–}101) + (10\text{–}1)]\}\\
&S'_{Ea0} = (1/\sqrt{6})\{(1\text{–}10) - (\text{–}110) + \varepsilon[(01\text{–}1) - (0\text{–}11)] + \varepsilon^*[(\text{–}101) - (10\text{–}1)]\}
\end{aligned}
$$

where $\varepsilon = \exp(i2\pi/3)$. The spin functions S_{Ebm} and S'_{Ebm} are obtained from the corresponding S_{Eam} and S'_{Eam} functions by interchanging ε and ε*. The functions for the negative values of m are analogous to those with positive m values when only 1 and –1 are interchanged.

It is worth realising that only some of the above spin functions are also eigenfunctions of the total spin, namely those with m = ±3, ±2 and S'_{A0}, S_{Ea0}, S'_{Ea0}, S_{Eb0}, and S'_{Eb0}, the others are not. However, they are simultaneous eigenfunctions of the rotational, Zeeman and the secular quadrupole Hamiltonians as far as $\omega_Q\tau < 1$. Furthermore, they are simple combinations and thus easy to use. At lower temperatures $\omega_Q\tau > 1$ the nonsecular quadrupole coupling mixes some of these functions. However, the spin functions (S1) can be still used, if all the A level populations can be described by one spin temperature T_A and the E level populations by another temperature T_E. Of course this is not exactly true because of the very slow spin diffusion. Nevertheless, it is approximately true, since all the A level polulations relax by practically identical rates, only the numerical factors vary somewhat (cf. Table SI). The same holds also for the E level populations.

The rotational wave functions for the rotational ground state are denoted R_{0A}, R_{0Ea} and R_{0Eb}.The products of the spin and rotational wave functions have to remain unchanged in the ±120 ° rotations of the methyl group about its axis. Therefore the spin–rotational wave functions Ψ are such products, where a spin function of the species A, E^a and E^b is multiplied by a A, E^b and E^a species rotational function, respectively. Thus the spin–rotational functions are $\Psi_{Am} = R_{0A}S_{Am}$, $\Psi_{Eam} = R_{0Eb}\,S_{Eam}$ and $\Psi_{Ebm} = R_{0Ea}\,S_{Ebm}$, where the spin function shows the irreducible index of the total spin–rotational function.

S2. Transition rates

The deuteron spin–lattice relaxation of CD_3 groups is dominated by the quadrupole interaction. When the largest value of the electric field gradient is assumed to be parallel to the C–D bond and the asymmetry parameter is taken equal to zero, the quadrupole interaction of the methyl deuteron u corresponds to the Hamiltonian (in angular frequency units)

$$H_{Qu} = \frac{1}{4}\omega_Q \sum_\mu B_u^{(\mu)} S_u^{(\mu)} \qquad \text{(S2)}$$

The lattice- and spin-dependent operators are defined by

$$\begin{aligned}
B_u^{(0)} &= 3\cos^2\theta_u - 1 \\
B_u^{(1)} &= \sin\theta_u\cos\theta_u\exp(-i\varphi_u) \\
B_u^{(2)} &= \sin^2\theta_u\exp(-i2\varphi_u) \\
S_u^{(0)} &= (1/2)(3I_{uz}^2 - I^2) \\
S_u^{(1)} &= (3/2)(I_{uz}I_{u+} + I_{u+}I_{uz}) \\
S_u^{(2)} &= (3/4)I_{u+}^2
\end{aligned} \qquad \text{(S3)}$$

The operators with the negative index –μ are $B_u^{(-\mu)} = B_u^{(\mu)*}$and $S_u^{(-\mu)} = S_u^{(\mu)*}$. The polar angles θ_u and φ_u define the orientation of the electric field gradient (now parallel to the C–D vector) in the laboratory frame, where the z axis shows the direction of the external magnetic field.

For the calculation of the transition rates between various spin–rotational wave functions the total quadrupole Hamiltonian is written in the symmetrised form

$$H_Q = H_{Qu} + H_{Qv} + H_{Qw} = \frac{1}{4}\omega_Q \sum_{\mu=0,\pm1,\pm2} \left(B_A^{(\mu)} S_A^{(\mu)} + B_{Eb}^{(\mu)} S_{Ea}^{(\mu)} + B_{Ea}^{(\mu)} S_{Eb}^{(\mu)} \right) \quad \text{(S4)}$$

where for example $B_{Eb}^{(\mu)} = (1/3)\left(B_u^{(\mu)} + \varepsilon B_v^{(\mu)} + \varepsilon^* B_w^{(\mu)} \right)$. $B_{Ea}^{(\mu)}$ is otherwise identical to $B_{Eb}^{(\mu)}$ but ε and ε^* are interchanged. The operators $S_{Ea}^{(\mu)}$ and $S_{Eb}^{(\mu)}$ are defined similarly but without the multiplier 1/3. The operators $B_A^{(\mu)} S_A^{(\mu)}$ are not modulated by the methyl rotation about its axis and are thus time-independent.

We calculated at first all the relevant matrix elements. The corresponding transition rates were then calculated from the time-dependent perturbation theory, for example

$$R_{E^b m' \leftrightarrow E^a m} = \frac{1}{8}\omega_Q^2 \left| \langle E^b m' \left| S_{Ea}^{(\mu)} \right| E^a m \rangle \right|^2 \left| B_{Eb}^{(\mu)} \right|^2 S(k_K, \mu\omega_0) \quad \text{(S5)}$$

with m' = m + μ, and the spectral density function defined by $S(k,\omega) = k/[k^2 + \omega^2]$. Actually the function $J(\tau_j,\omega)$ used in Eq. (1) is identical to $S(k,\omega)$ when τ_j is replaced by $1/k$. The quantity k_K is the damping rate of the so-called Kramers coherence, which is related to pairs of spin–rotational E levels at ground and excited rotational states [24, 25]. Similarly, k_t is the damping rate of the tunnelling coherence, which involves pairwise an A level and an E^a (or E^b) level. It is important in the relaxation transitions between the A and E levels, which involve a change also in the tunnelling energy. The rates k_K and k_t were shown to be equal to the broadening of the quasielastic $E^a \leftrightarrow E^b$ and inelastic A ↔ E tunnelling lines in inelastic neutron scattering experiments, respectively [11, 37]. There are altogether 14 basically different transition rates. Eight of them are defined by

$$\begin{aligned}
R_{K0} &= \frac{9}{2}\omega_Q^2 \left| B_{Ea}^{(0)} \right|^2 S(k_K, \Delta\omega_Q) \\
R_{Ka1} &= \frac{9}{32}\omega_Q^2 \left| B_{Ea}^{(-1)} \right|^2 S(k_K, \omega_0) \\
R_{Ka2} &= \frac{9}{64}\omega_Q^2 \left| B_{Ea}^{(-2)} \right|^2 S(k_K, 2\omega_0) \\
R_{t0} &= \frac{9}{2}\omega_Q^2 \left| B_{Ea}^{(0)} \right|^2 S(k_t, \omega_t) \\
R_{ta\pm1} &= \frac{9}{32}\omega_Q^2 \left| B_{Ea}^{(-1)} \right|^2 S(k_t, \omega_t \pm \omega_0) \\
R_{ta\pm2} &= \frac{9}{64}\omega_Q^2 \left| B_{Ea}^{(-2)} \right|^2 S(k_t, \omega_t \pm 2\omega_0)
\end{aligned} \quad \text{(S6)}$$

The subindex K or t defines the damping rate k_K or k_t appearing in the spectral density function. In addition t means that the tunnel frequency ω_t is included. The index a defines the symmetry of the lattice–dependent function $B_{Ea}^{(-\mu)}$, while the last index, equal to ±1 or ±2, shows the multiplier of ω_0. The remaining rates R_{Kb1}, R_{Kb2}, etc. are obtained from (S6) by replacing $B_{Ea}^{(-\mu)}$ by $B_{Eb}^{(-\mu)}$. Since $B_{Ea}^{(0)*} = B_{Eb}^{(0)}$, the subindex a or b is not needed in R_{K0} and R_{t0}. The frequency $\Delta\omega_Q$ is roughly equal to $\left| B_{Ea}^{(0)} \right|$. All the transition rates between the spin–rotational levels can be expressed in terms of these basic rates as shown in Table SI.

The angular dependence of the rates can be obtained from Ref. 26. That study considered ^{13}C relaxation related to the magnetic dipolar interaction between ^{13}C and H nuclei in $^{13}CH_3$ compounds. Since the angles between the ^{13}C–H vectors are the same

tetrahedral angles as those between C–D vectors (each parallel to the principal axis of the deuteron quadrupole interaction), the results presented in Table 3 of Ref. 26 give the angular dependence of $\left|B_{Ea}^{(-1)}\right|^2$ and $\left|B_{Ea}^{(-2)}\right|^2$ in (S6).

It should be noticed that we do not make any difference between the upwards and downwards transitions. This is justified as far as deviations from thermal equilibrium are considered and the tunnelling frequency ω_t is much smaller than the thermal energy. That requirement is well fulfilled in the present study, where the experiments were conducted above 5 K.

Table SI. The transition rates from the states E^a (called initial) to A and E^b (called final states). The opposite rates are the same when $kT >> \omega_t$. In addition to the shown rates, there are transition rates between E^b and A states, which are otherwise identical to those in the lower part of the table but with the subindices a and b interchanged.

Final state	Initial state							
	E^a2	E^a1	E^a0	E^a-1	E^a-2	E^a1'	E^a0'	E^a-1'
E^b2	R_{K0}	$2R_{Ka1}$	R_{Ka2}	–	–	$8R_{Ka1}$	$3R_{Ka2}$	–
E^b1	$2R_{Kb1}$	–	R_{Ka1}	$8R_{Ka2}$	–	–	$3R_{Ka1}$	–
E^b0	R_{Kb2}	R_{Kb1}	R_{K0}	R_{Ka1}	R_{Ka2}	$4R_{Kb1}$	–	$4R_{Ka1}$
E^b-1	–	$8R_{Kb2}$	R_{Kb1}	–	$2R_{Ka1}$	–	$3R_{Kb1}$	–
E^b-2	–	–	R_{Kb2}	$2R_{Kb1}$	R_{K0}	–	$3R_{Kb2}$	$8R_{Kb1}$
E^b1'	$8R_{Kb1}$	–	$4R_{Ka1}$	–	–	R_{K0}	–	$2R_{Ka2}$
E^b0'	$3R_{Kb2}$	$3R_{Kb1}$	–	$3R_{Ka1}$	$3R_{Ka2}$	–	R_{K0}	–
E^b-1'	–	–	$4R_{Kb1}$	–	$8R_{Ka1}$	$2R_{Kb2}$	–	R_{K0}
A3	$6R_{tb1}$	$6R_{tb2}$	–	–	–	–	–	–
A2	R_{t0}	$2R_{tb1}$	R_{tb2}	–	–	$2R_{tb1}$	$3R_{tb2}$	–
A1	$2R_{ta-1}$	–	$4R_{tb1}$	$2R_{tb2}$	–	–	–	–
A0	R_{ta-2}	R_{ta-1}	R_{t0}	R_{tb1}	R_{tb2}	R_{ta-1}	–	R_{tb1}
A −1	–	$2R_{ta-2}$	$4R_{ta-1}$	–	$2R_{tb1}$	–	–	–
A −2	–	–	R_{ta-2}	$2R_{ta-1}$	R_{t0}	–	$3R_{ta-2}$	$2R_{ta-1}$
A −3	–	–	–	$6R_{ta-2}$	$6R_{ta-1}$	–	–	–
A1'	$2R_{ta-1}$	–	R_{tb1}	–	–	R_{t0}	$3R_{tb1}$	$2R_{tb2}$
A0'	$3R_{ta-2}$	$3R_{ta-1}$	–	$3R_{tb1}$	$3R_{tb2}$	$3R_{ta-1}$	R_{t0}	$3R_{tb1}$
A −1'	–	–	R_{ta-1}	–	$2R_{tb1}$	$2R_{ta-2}$	$3R_{ta-1}$	R_{t0}
A0"	–	–	–	–	–	$6R_{ta-1}$	–	$6R_{tb1}$

S3. Relaxation rate of the deuteron magnetisation

The deuteron magnetisation, without the multiplier $\gamma\hbar$, is equal to

$$M = 3(\mathrm{N_{A3}} - \mathrm{N_{A-3}}) + 2(\mathrm{N_{A2}} - \mathrm{N_{A-2}}) + 2(\mathrm{N_{Ea2}} - \mathrm{N_{Ea-2}}) + 2(\mathrm{N_{Eb2}} - \mathrm{N_{Eb-2}}) + (\mathrm{N_{A1}} - \mathrm{N_{A-1}}) + (\mathrm{N'_{A1}} - \mathrm{N'_{A-1}}) + (\mathrm{N_{Ea1}} - \mathrm{N_{Ea-1}}) + (\mathrm{N'_{Ea1}} - \mathrm{N'_{Ea-1}}) + (\mathrm{N_{Eb1}} - \mathrm{N_{Eb-1}}) + (\mathrm{N'_{Eb1}} - \mathrm{N'_{Eb-1}}) \quad \text{(S7)}$$

where the level populations are indexed according to the spin states (1). Usually the magnetisations
$M_\mathrm{A} = 3(\mathrm{N_{A3}} - \mathrm{N_{A-3}}) + 2(\mathrm{N_{A2}} - \mathrm{N_{A-2}}) + (\mathrm{N_{A1}} - \mathrm{N_{A-1}}) + (\mathrm{N'_{A1}} - \mathrm{N'_{A-1}})$ and M_E (containing the remaining terms of (S7)) are expected to relax at different rates and therefore we consider them separately. There are altogether 26 independent populations. Therefore, in addition to the magnetisations M_A and M_E there are 24 other independent population combinations [11]. The number of remaining combinations is greatly reduced, if we can assume two spin temperatures, T_A for the A species populations and T_E for the E species combinations. Of course this is most likely not exactly true because of the slow spin diffusion between deuterons of neighbouring methyl groups. However, a closer look at the transition rates in Table SI reveals that all the A species populations relax by practically identical transition rates, only the numerical multipliers are somewhat different. The same holds for the E species populations. Therefore, the assumption of the two spin temperatures should be anyway a reasonable one. Most of the remaining independent combinations relax much faster than M_A and M_E since the dominant transition rates do not depend on ω_0 or ω_t. Also the quadrupole order belongs to them. After that we are left with two, the tunnelling reservoir and the rotational polarization, which can influence the magnetization relaxation. The tunnelling reservoir relaxes rather slowly while the rotational polarization relaxes often faster than M_A and M_E, only in the fast-motion regime $\omega_0\tau < 1$ the latter relaxes roughly at the same rate as the two magnetizations [11]. Therefore it can alter the magnetization relaxation only at such temperatures. Since all the rates (S6) are of the same magnitude under such conditions, the relaxation rates of M_A and M_E cannot be significantly altered. Therefore, we consider only the coupling to the tunnelling reservoir in the following. The tunnelling reservoir means the excess of A level populations relative to the E level populations. This reservoir is not affected by a saturation of one 90° rf pulse (or a short burst of 90° pulses). Therefore, it does not affect the initial relaxation of M_A and M_E although it can modify these magnetisations during later stages of relaxation especially near level crossings $\omega_\mathrm{t} = \omega_0$ and $\omega_\mathrm{t} = 2\omega_0$. Below we show that the initial relaxation rates of M_A and M_E after a short saturating sequence describe also the later relaxation with reasonable accuracy. In the level-crossing region of ω_t roughly equal to ω_0 the initial relaxation rates will be somewhat modified.

The various terms of the time derivatives $\mathrm{d}M_\mathrm{A}/\mathrm{d}t$ and $\mathrm{d}M_\mathrm{E}/\mathrm{d}t$ can be calculated by using the transition rates of Table SI and the method explained for example in Ref. 26. The results turn out to be

$$\mathrm{d}\Delta M_\mathrm{A}/\mathrm{d}t = -R_\mathrm{A}\Delta M_\mathrm{A} + R_\mathrm{AE}\Delta M_\mathrm{E}$$

$$\mathrm{d}\Delta M_\mathrm{E}/\mathrm{d}t = R_\mathrm{EA}\Delta M_\mathrm{A} - R_\mathrm{E}\Delta M_\mathrm{E} \quad \text{(S8)}$$

with

$$R_{\mathrm{A}} = (1/15)[10R_{\mathrm{t0}} + 41(R_{\mathrm{ta1}} + R_{\mathrm{ta-1}} + R_{\mathrm{tb1}} + R_{\mathrm{tb-1}}) + 37(R_{\mathrm{ta2}} + R_{\mathrm{ta-2}} + R_{\mathrm{tb2}} + R_{\mathrm{tb-2}})]$$

$$R_{\mathrm{E}} = (1/12)[10R_{\mathrm{t0}} + 18(R_{\mathrm{Ka1}} + R_{\mathrm{Kb1}}) + 36(R_{\mathrm{Ka2}} + R_{\mathrm{Kb2}}) + 29(R_{\mathrm{ta1}} + R_{\mathrm{ta-1}} + R_{\mathrm{tb1}} + R_{\mathrm{tb-1}}) + 13(R_{\mathrm{ta2}} + R_{\mathrm{ta-2}} + R_{\mathrm{tb2}} + R_{\mathrm{tb-2}})]$$

$$12R_{\mathrm{AE}} = 15R_{\mathrm{EA}} = 10R_{\mathrm{t0}} + 26(R_{\mathrm{ta1}} + R_{\mathrm{ta-1}} + R_{\mathrm{tb1}} + R_{\mathrm{tb-1}}) + 7(R_{\mathrm{ta2}} + R_{\mathrm{ta-2}} + R_{\mathrm{tb2}} + R_{\mathrm{tb-2}})$$

(S9)

It should be noticed that M_{A} and M_{E} are generally coupled to the tunnelling reservoir although the coupling terms are not shown in (S8). The difference magnetisations are deviations from the thermal equilibrium value, for example $\Delta M_{\mathrm{A}} = M_{\mathrm{A}} - M_{\mathrm{A}}(\mathrm{eq})$. In thermal equilibrium the spin temperatures are equal and $M_{\mathrm{A}}(\mathrm{eq}) = (5/9)M(\mathrm{eq})$ and $M_{\mathrm{E}}(\mathrm{eq}) = (4/9)M(\mathrm{eq})$, where $M(\mathrm{eq})$ is the total magnetisation of the methyl deuterons.

Eqs. (S8) lead to a biexponential relaxation, the magnetisations M_{A} and M_{E} relaxing at different rates. Our calculations show that for large tunnel splittings $\omega_{\mathrm{t}} > \omega_0$ not only the coupling of the total magnetization $M_{\mathrm{A}} + M_{\mathrm{E}}$ to the tunnelling reservoir vanishes [11] but also M_{A} and M_{E} become separately uncoupled from it. Since R_{E} is much larger than the other rates in (S9) in the slow motion region, the deuterons of the E species methyl groups relax quite accurately at the rate R_{E}, which is practically equal to the initial relaxation rate R_{Ein} (S10). Then ΔM_{E} is vanishingly small during the relaxation of the magnetization M_{A} and therefore M_{A} will relax exponentially at the rate R_{A}, which is roughly equal to R_{Ain}. Since the equilibrium magnetizations obey $M_{\mathrm{A}}(\mathrm{eq}) = (5/4)M_{\mathrm{E}}(\mathrm{eq})$, the initial relaxation rates, after the saturation of the deuteron magnetization, are

$$R_{\mathrm{Ain}} = R_{\mathrm{A}} - (4/5)R_{\mathrm{AE}} = R_{\mathrm{ta1}} + R_{\mathrm{ta-1}} + R_{\mathrm{tb1}} + R_{\mathrm{tb-1}} + 2R_{\mathrm{ta2}} + 2R_{\mathrm{ta-2}} + 2R_{\mathrm{tb2}} + R_{\mathrm{tb-2}}$$

$$R_{\mathrm{Ein}} = R_{\mathrm{E}} - (5/4)R_{\mathrm{EA}} = (1/4)[6(R_{\mathrm{Ka1}} + R_{\mathrm{Kb1}}) + 12(R_{\mathrm{Ka2}} + R_{\mathrm{Kb2}}) + R_{\mathrm{ta1}} + R_{\mathrm{ta-1}} + R_{\mathrm{tb1}} + R_{\mathrm{tb-1}} + 2R_{\mathrm{ta2}} + 2R_{\mathrm{ta-2}} + 2R_{\mathrm{tb2}} + 2R_{\mathrm{tb-2}}]$$

(S10)

If $\omega_{\mathrm{t}} < \omega_0$, the rates coupling M_{A} and M_{E} to the tunnelling reservoir are much smaller than the rates (S9) and the relaxation seems to be biexponential. However, the terms $\mathrm{B}_{\mathrm{Ea}}^{(0)}\mathrm{S}_{\mathrm{Eb}}^{(0)}$ and $\mathrm{B}_{\mathrm{Eb}}^{(0)}\mathrm{S}_{\mathrm{Ea}}^{(0)}$ of the quadrupole Hamiltonian (S4) cause transitions at a relatively large rate R_{t0} from $\mathrm{A_m}$ to $\mathrm{E}_{\mathrm{m}}^{\mathrm{a}}$ and $\mathrm{E}_{\mathrm{m}}^{\mathrm{b}}$ levels and backwards (Table SI). Furthermore, they cause transitions between $\mathrm{E}_{\mathrm{m}}^{\mathrm{a}}$ and $\mathrm{E}_{\mathrm{m}}^{\mathrm{b}}$ at the rate R_{K0}, which exceeds the other rates (S6) except in the fast-motion regime. Thus the difference between the E^{a} and E^{b} level populations may have a small effect in this region, but considering the accuracy of the present method it can be rather safely ignored. Then the relaxation rates of M_{A} and M_{E} approach each other and the common initial relaxation rate. The rates R_{Ain} and R_{Ein} are indeed equal, if the damping rates k_{K} and k_{t} are equal and $\omega_{\mathrm{t}} < \omega_0$.

When the tunnel and resonance frequencies are of the same magnitude, then the coupling between M_A and M_E and to the tunnel reservoir becomes important. This leads to 3x3 determinants for eigenrates and corresponding weights. It is known that the smallest eigenrate does not show any maxima at the level crossings $\omega_t = \omega_0$ and $\omega_t = 2\omega_0$ but varies smoothly through them [11]. Both R_{Ain} and R_{Ein} show strong maxima at the level crossings although one of them should vary smoothly. To remove this discrepancy we require that whenever the differences $|\omega_t - \omega_0|$ and $|\omega_t - 2\omega_0|$ are smaller than $\omega_0/2$ we replace them by $\omega_0/2$ in the denominators of R_{ta-1}, R_{tb-1}, R_{ta-2} and R_{tb-2} when calculating the rate R_{Ain}. [Such a replacement is not done in the calculations of R_{Ein}; there the lower limit for the differences $|\omega_t - \omega_0|$ and $|\omega_t - 2\omega_0|$ is taken equal to 160 kHz, because the quadrupole coupling makes the smallest distance between the apparently crossing levels roughly equal to the strength of the coupling.] The described method is only qualitatively true, but because the number of methyl groups having ω_t between $\omega_0/2$ and $5\omega_0/2$ is relatively small in the case of a broad distribution of activation energies and potential strengths, the accuracy of the obtained results should not be significantly degraded. Of course one could in principle continue according to Ref. [11], take into account the couplings to the tunnelling reservoir and the rotational polarization and include their effect in numerical calculations, at the expense of remarkably increased computing work. Unfortunately even this would not necessarily lead to more accurate results, because the lack of spin diffusion invalidates the underlying implicit assumptions concerning the population relations also in [11].

The angular dependence of (S10) is obtained from Table 3 of Ref. 26 or Table 1 of Ref. 38, the latter table including also the averaging effect of fast torsional oscillations. By neglecting the torsional averaging we obtain [26]

$$\left|B_{Ea}^{(-1)}\right|^2 + \left|B_{Eb}^{(-1)}\right|^2 = \frac{4}{81}\left[3 - 3c^2 + 2c^4 + 4\sqrt{2}ac(a^2 - 3b^2)\right] = \frac{4}{81}\mathrm{Ang}_1$$

$$\left|B_{Ea}^{(-2)}\right|^2 + \left|B_{Eb}^{(-2)}\right|^2 = \frac{8}{81}\left[3 + 6c^2 - c^4 - 2\sqrt{2}ac(a^2 - 3b^2)\right] = \frac{8}{81}\mathrm{Ang}_2 \qquad \text{(S11)}$$

Here $a = \sin\theta_m\cos\phi_m$, $b = \sin\theta_m\sin\phi_m$ and $c = \cos\theta_m$ are the direction cosines of the methyl axis relative to the laboratory frame (with the z axis parallel to the external magnetic field) and θ_m and ϕ_m are the corresponding polar and phase angles. When Eqs. (S11) and (S6) are inserted into (S9), the initial relaxation rates become

$$R_{Ain} = (1/72)\omega_Q^2\{\mathrm{Ang}_1[S(k_t, \omega_t + \omega_0) + S(k_t, \omega_t - \omega_0)] + 2\mathrm{Ang}_2[S(k_t, \omega_t + 2\omega_0) + S(k_t, \omega_t - 2\omega_0)]\}$$

$$R_{Ein} = (1/288)\omega_Q^2\{\mathrm{Ang}_1[6S(k_K, \omega_0) + S(k_t, \omega_t + \omega_0) + S(k_t, \omega_t - \omega_0)] + \mathrm{Ang}_2[12S(k_K, 2\omega_0) + 2S(k_t, \omega_t + 2\omega_0) + 2S(k_t, \omega_t - 2\omega_0)]\} \qquad \text{(S12)}$$

It is worth realising that if the coherence damping rates k_t and k_K are equal and $\omega_t << \omega_0$, then the rates R_{Ain} and R_{Ein} become equal. These also agree with the results of Diezemann et al. [10, 11]. The result of Pratt and co-workers [5, 17] does not contain the orientation–dependent term $ac(a^2–3b^2)$, which takes into account the threefold symmetry of the methyl group. Its average value vanishes for polycrystalline samples and thus removes the discrepancy between their result and the present study for powders.